



# **A parametric study on the evolution of cyclic clay-pile interface friction for large numbers of cycles**

Rawaz Dlawar Muhammed, Jean Canou, Jean-Claude Dupla, Alain Tabbagh

## **► To cite this version:**

Rawaz Dlawar Muhammed, Jean Canou, Jean-Claude Dupla, Alain Tabbagh. A parametric study on the evolution of cyclic clay-pile interface friction for large numbers of cycles. Geotechnical and Geological Engineering, 2020, 10.1007/s10706-020-01377-4 . hal-03837942

**HAL Id: hal-03837942**

**<https://hal.science/hal-03837942>**

Submitted on 3 Nov 2022

**HAL** is a multi-disciplinary open access archive for the deposit and dissemination of scientific research documents, whether they are published or not. The documents may come from teaching and research institutions in France or abroad, or from public or private research centers.

L'archive ouverte pluridisciplinaire **HAL**, est destinée au dépôt et à la diffusion de documents scientifiques de niveau recherche, publiés ou non, émanant des établissements d'enseignement et de recherche français ou étrangers, des laboratoires publics ou privés.

# Geotechnical and Geological Engineering

## A parametric study on the evolution of cyclic clay-pile interface friction for large numbers of cycles --Manuscript Draft--

Manuscript Number:	GEGE-D-19-00647
Full Title:	A parametric study on the evolution of cyclic clay-pile interface friction for large numbers of cycles
Article Type:	Original Research
Keywords:	Pile behavior; local shaft friction; amplitude of cyclic loading; frequency, confining effective stress; saturated clay; physical modelling; instrumented pile-probe
Corresponding Author:	Rawaz Dlawar Muhammed, Ph.D. Ecole des Ponts ParisTech Champs-sur-Marne, FRANCE
Corresponding Author Secondary Information:	
Corresponding Author's Institution:	Ecole des Ponts ParisTech
Corresponding Author's Secondary Institution:	
First Author:	Rawaz Dlawar Muhammed, Ph.D.
First Author Secondary Information:	
Order of Authors:	Rawaz Dlawar Muhammed, Ph.D.
	Canou Jean, Ph.D.
	Jean-Claude Dupla, Ph.D.
	Alain Tabbagh, Ph.D.
Order of Authors Secondary Information:	
Funding Information:	
Abstract:	<p>In this paper, an experimental study is presented investigating the influence of cyclic displacement amplitude and effective consolidation stress on the evolution of mobilized local shaft friction along piles submitted to large number of cycles (up to 10<sup>5</sup> cycles). Two-way cyclic displacement-controlled tests were performed on an instrumented pile-probe installed and loaded in a calibration chamber. Tests were performed on reconstituted specimens of saturated clay to examine the shaft friction evolution in the soil-pile interface during cyclic loading. Displacement-controlled static tests were also performed before and after the cyclic loading in order to quantify the influence of cyclic parameters on post-cyclic static response. It was found that the amplitude of cyclic displacement and the initial state of stress have an influence on the evolution of local friction during cyclic loading. The degradation rate of local friction increased for larger cyclic displacement amplitudes whereas with increasing the effective consolidation stress, the degradation rate decreased. The application of displacement- controlled cycles resulted in a modification in the behavior of the interface. A significant peak of static friction followed by strain softening was observed during post cyclic static tests, which was not the case for pre-cyclic static tests. The peak value of friction obtained upon post-cyclic static loadings found to be more important for higher values of applied displacement amplitude during cyclic loading. Finally, a brief synthesis of the results is presented.</p>
Suggested Reviewers:	Daniel Levacher, Dr. Professeur, Universite de Caen Normandie daniel.levacher@unicaen.fr He has extensive knowledge and skills to review this article.
	Pierre Breul, Dr

	Professor, Universite Clermont Auvergne et associes pierre.breul@uca.fr
	Mark Randolph mark.randolph@uwa.edu.au
	Rodrigo Salgado, Ph.D. Professor rodrigo@purdue.edu

[Click here to view linked References](#)

# A parametric study on the evolution of cyclic clay-pile interface friction for large numbers of cycles

Rawaz Dlawar Muhammed<sup>1,2</sup>, Jean Canou<sup>1</sup>, Jean-Claude Dupla<sup>1</sup>, Alain Tabbagh<sup>2</sup>

<sup>1</sup> *Ecole des Ponts ParisTech, Navier laboratory, France*

<sup>2</sup> *Pierre and Marie Curie University, France*

## **Corresponding Author:**

Rawaz Dlawar Muhammed

Ecole des Ponts – ParisTech, Navier laboratory

6 – 8 avenue Blaise Pascal, Cité Descartes, Champs-sur-Marne,

77455 Marne-La-Vallée, France

Phone : +33 1 64 15 35 46

Email: rawaz-dlawar.muhammed@enpc.fr

## ABSTRACT:

In this paper, an experimental study is presented investigating the influence of cyclic displacement amplitude and effective consolidation stress on the evolution of mobilized local shaft friction along piles submitted to large number of cycles (up to  $10^5$  cycles). Two-way cyclic displacement-controlled tests were performed on an instrumented pile-probe installed and loaded in a calibration chamber. Tests were performed on reconstituted specimens of saturated clay to examine the shaft friction evolution in the soil-pile interface during cyclic loading. Displacement-controlled static tests were also performed before and after the cyclic loading in order to quantify the influence of cyclic parameters on post-cyclic static response. It was found that the amplitude of cyclic displacement and the initial state of stress have an influence on the evolution of local friction during cyclic loading. The degradation rate of local friction increased for larger cyclic displacement amplitudes whereas with increasing the effective consolidation stress, the degradation rate decreased. The application of displacement- controlled cycles resulted in a modification in the behavior of the interface. A significant peak of static friction followed by strain softening was observed during post cyclic static tests, which was not the case for pre-cyclic static tests. The peak value of friction obtained upon post-cyclic static loadings found to be more important for higher values of applied displacement amplitude during cyclic loading. Finally, a brief synthesis of the results is presented.

## KEY WORDS:

Pile behavior, local shaft friction, amplitude of cyclic loading, frequency, confining effective stress, saturated clay, physical modelling, instrumented pile-probe

## 1 – INTRODUCTION

During their lifetime, pile foundations are often subjected, in addition to permanent static loads, to variable transient loadings, which will sometimes modify their bearing capacity. These complex loadings, often identified under the generic term of “cyclic loadings”, can be characterized by various parameters like the amplitude of the cycles, their frequency, regularity, number of cycles, length of the sequences, etc. Understanding the behavior of piles submitted to such cyclic loadings constitutes an important aspect to be taken into account in the design of pile foundations. Over the past few decades, this subject has attracted considerable scientific interest and numerous research work has been published focusing on pile behavior under cyclic loading (Chan and Hanna (1980), Lee and Poulos (1990), Al-Douri and Poulos (1995), Chin and Poulos (1996), Le Kouby et al. (2004), Lehane and White (2004), Tsuha et al. (2012), Poulos (1981), Matlock et al. (1988), Goulois et al. (1985) or Procter and Khaffaf (1987)).

In most laboratory studies based on the use of physical modelling approach of pile-soil interface behavior, the authors usually applied displacement-controlled cyclic loading on their pile, which seems to be the appropriate way to study the evolution of local interface soil-pile friction (ex. Matlock et al. (1982), Poulos (1981), Procter and Khaffaf (1987), Bekki *et al.* (2013), Muhammed *et al.* (2018a)).

Reported studies in the literature showed that the mechanical behavior of the soil–pile interface depends on various parameters like soil, interface and loading parameters. Poulos (1981) conducted a number of small-scale laboratory tests on a model pile section (20 mm in diameter) in reconstituted saturated clay specimens (152 mm in diameter), up to maximum number of 1000 cycles. According to this author, no degradation of skin friction occurs unless the half-amplitude of the cyclic displacement exceeds about 0.2% of the diameter. Above this value, increasing cyclic displacement amplitude leads to degradation and loss of skin friction. The amplitude of cyclic displacement required to initiate degradation may vary considerably from one test to another. Poulos (1981) and Lee and Poulos (1993) indicated that the critical amplitude of cyclic displacement, at which cyclic degradation is initiated, is related to the displacement required for full friction mobilization in a static load test.

All laboratory test results published to date regarding the evolution of local soil-pile interface friction upon cyclic loadings for clays only address small to medium numbers of cycles, less than  $10^4$  cycles. To the authors’ knowledge, there are no published data showing the influence of cyclic parameters on the evolution of saturated clay-pile local friction for large numbers of cycles. However, in several cases, the foundation of structures can be exposed to cycles of loadings that can exceed  $10^4$  cycles (ex. offshore wind pile foundation). Investigating the evolution of local pile friction upon large number of cycles is therefore an important issue for better understanding the behavior of piles.

Within this context, this paper presents the results of an experimental study aimed at better understanding the frictional behavior of a clay-pile interface under large number of cycles. The approach used is of the physical modelling type, using an instrumented prototype probe tested in a calibration chamber and loaded under various types of monotonic and cyclic loadings.

Based on the results obtained, the influence of cyclic displacement amplitude as well as initial effective consolidation stress of the specimen, on the evolution of mobilized local shaft friction along the probe is investigated for large numbers of cycles (up to  $10^5$  cycles). Subsequently, the

effects of the cyclic sequences on the post-cyclic static response of the pile are presented and discussed.

## 2 – TESTING SETUP, EXPERIMENTAL PROTOCOLS AND SOIL USED

The tests presented in this paper have been performed in the calibration chamber available in the geotechnical team of Navier laboratory at Ecole des Ponts ParisTech. The clay specimen is first reconstituted in a large size consolidometer and then transferred onto the calibration chamber for final consolidation. The corresponding detailed experimental protocols used for specimen preparation, application of stresses in the calibration chamber and for carrying out the loading tests with the pile-probe have been fully described by Muhammed (2015), Muhammed *et al.* (2018a and 2018b) and Muhammed *et al.* (2019), who also report on the design of the instrumented pile-probe and the consolidometer. Therefore, a brief description only of the experimental setup and testing protocol is given in the following.

### 2.1 - The calibration chamber testing setup

A 3D drawing of the calibration chamber test set-up is shown in Fig. 1. The chamber can hold soil specimens 700 mm high and 524 mm in diameter. Independent vertical and horizontal stresses may be applied to the specimens. This allows to apply isotropic or anisotropic initial states of stress or  $K_0$  conditions to the specimens, thus simulating the state of stress applied to a soil element at a given depth. The loading frame of the chamber is equipped with a long stroke classical 100 kN hydraulic jack, used for probe installation at constant displacement rate, and with a servohydraulic 100 kN actuator for carrying out precise displacement-controlled or force-controlled monotonic and cyclic loadings.

### 2.2 - Large size consolidometer for reconstituting specimens of saturated fine-grained soils

The consolidometer setup allows to reconstitute, starting from a slurry, saturated clay specimens 524 mm in diameter and 600 to 800 mm high under  $K_0$  conditions (no lateral deformation is allowed during the consolidation process). The reservoir of the consolidometer is composed of two Plexiglas adjustable rigid halves equipped with top and bottom draining plates. A loading frame equipped with a double-action hydraulic jack, powered by a hydro-pneumatic pump, allows the application, during the consolidation process, of constant force increments on the top plate of the specimen. Fig. 2 shows a 3D drawing of the consolidometer set-up.

### 2.3 - The instrumented pile-probe

The prototype probe used allows to make direct and independent measurements of tip resistance and local shaft friction representative of values occurring along a pile shaft. The probe has a cross section of 10 cm<sup>2</sup> (diameter of 36 mm), similar to standard penetrometers. The conical tip

of the probe is equipped with a 20 kN precision force transducer and the sleeve, 11 cm long (sleeve surface of 124.4 cm<sup>2</sup>), is equipped with a  $\pm 5$  kN force transducer. The bottom part of the probe, including the friction sleeve, is threaded horizontally in order to provide a perfectly rough interface surface state with respect to friction mobilization. The average roughness of the rough part is  $R_a = 0.4 \mu\text{m} \pm 0.25$ . Fig. 3 shows a simplified cross section of the probe, together with different views.

## 2.4 - Experimental procedure

### *Specimen reconstitution*

The specimen preparation comprises two main steps: (1) the specimen is first pre-consolidated in the consolidometer, starting from a clay slurry, to a predefined value of vertical stress, under  $K_0$  conditions; (2) the pre-consolidated specimen is then transferred and positioned on the bottom piston of the calibration chamber and consolidated to the final consolidation stress. The initial water content of the clay slurry has been fixed to about 1.7 times its liquid limit (Muhammed *et al.* (2018a)). The consolidation of the specimen in the consolidometer is achieved by progressively increasing the vertical load by increments (5, 15, 45, 125, 250, ...kPa) up to the maximum preselected value of the vertical load.

Once the consolidation process has been completed, the pre-consolidated specimen is transported and carefully adjusted on the bottom piston of the calibration chamber. The consolidation reservoir is taken out and a rubber membrane is adjusted around the clay specimen. The circular confinement wall is then adjusted around the specimen. The final state of consolidation stress can then be slowly applied to the specimen, by increasing independently the vertical pressure within the piston chamber and the lateral confinement pressure. This allows to follow an anisotropic consolidation stress path as the state of stress initially applied in the consolidometer. Further details about the experimental procedure used can be found in Muhammed *et al.* (2018a).

### *Loading protocol*

A given test is composed of different successive sequences listed below:

- (i) Installation of the pile-probe at constant displacement rate (1 mm/s) with the long stroke hydraulic jack;
- (ii) Pre-cyclic static displacement-controlled loading tests up to failure;
- (iii) Cyclic displacement-controlled sequence;
- (iv) Post-cyclic static displacement-controlled loading tests up to failure.

## 2.5 - Tested soil

The tests presented in this paper have been carried out on saturated specimens of kaolinite Speswhite. The physical properties of this reference clay, as determined by the authors, are



1 listed in table 1. The particle size distribution curve of the deflocculated Speswhite clay is  
2 shown in Fig. 4.  
3  
4

### 5 **3 – PRESENTATION OF A TYPICAL TEST**

6  
7

8 A typical test is presented in this section. For this test (Test 1), the initial consolidation of the  
9 specimen has been achieved in five steps in the consolidometer, corresponding to successive  
10 vertical stresses of 5, 15, 45, 125 and 250 kPa. Then, the pre-consolidated clay specimen has  
11 been placed in the calibration chamber and submitted to a final vertical effective stress  $\sigma'_{v0}$  of  
12 250 kPa and a final effective horizontal stress  $\sigma'_{h0}$  of 150 kPa corresponding to an estimated  
13 value of  $K_0$  equal to 0.59. The permeability and consolidation coefficient of the clay under this  
14 state of stress have been determined based on oedometer tests, giving  $k = 2.7 \cdot 10^{-9}$  m/s and  
15  $c_v = 3.0 \cdot 10^{-7}$  m<sup>2</sup>/s.  
16  
17  
18  
19  
20

#### 21 **3.1 - Installation of the pile-probe**

22  
23

24 The probe is initially pushed into the clay specimen with a constant penetration rate of 1 mm/s  
25 down to a penetration depth of 460 mm. This depth corresponds to a position of the probe for  
26 which the friction sleeve is practically vertically centered in the clay specimen. Measurements  
27 of tip resistance, local skin friction and total load head versus probe penetration during the  
28 installation sequence are presented in Fig. 5. The tip resistance mobilization is fairly rapid and  
29 a plateau is reached after 180 mm of tip penetration. The mobilization of local friction starts  
30 when the sleeve friction gets into the soil specimen at about 250 mm of tip penetration after  
31 which it increases progressively and reaches an almost stabilized steady state value.  
32 This stabilization of tip resistance and local skin friction accounts for a good homogeneity of  
33 the clay within the reconstituted specimen, thus validating the specimen preparation protocol.  
34 As far as the total head load is concerned, which accounts for the global mobilization of both  
35 tip resistance and friction along the probe shaft, a rapid increase is first observed up to 50 mm  
36 of the penetration depth. This rapid increase corresponds to the rapid mobilization of tip  
37 resistance. Then, a second phase of increase with a lower rate is observed accounting for the  
38 progressive increase of the friction surface in the sample.  
39  
40  
41  
42  
43  
44

45 During all sequences of a given test, results of tip resistance, local friction and total head load  
46 are systematically recovered. This provides fairly good confidence with respect to the measured  
47 local values (tip and friction) since at any stage of the test, the values obtained in terms of local  
48 friction and tip resistance can be validated by the total head load measurements. However, as  
49 mentioned in the objectives of the paper, the focus will mainly be on results concerning local  
50 friction in the following.  
51  
52  
53

#### 54 **3.2 - Pre-cyclic static loading of the probe**

55  
56

57 The pre-cyclic static (monotonic) loading tests are carried out in order to obtain the failure  
58 characteristics in terms of local friction and tip resistance. Two successive displacement-  
59 controlled static loadings are performed after full dissipation of the excess pore water generated  
60  
61  
62  
63  
64  
65

during pile installation (the probe is left unloaded before static tests for at least 12 hours). The first loading is performed at a displacement rate of 30  $\mu\text{m}/\text{min}$  while the second one is performed at a rate of 300  $\mu\text{m}/\text{min}$  (Fig. 6). A two hours rest was permitted after the first loading.

A very rapid mobilization of local friction, followed by a plateau, was obtained in both cases (about 34 kPa). Similar results were reported by Mochtar and Edil (1988) for a model pile tested in a saturated kaolinitic clay with similar characteristics. It is interesting to note that the results obtained in terms of failure characteristics are very similar for both tests and that the second loading is not significantly affected by the first one. It is also worth mentioning that the local friction mobilized upon initial static tests is almost two times higher than the friction mobilized during installation of the probe. This can be explained by the fact that during the installation phase, very high values of excess pore water pressure (EPWP) can be generated due to full displacement process, which reduces significantly the normal effective stress level acting at the soil-probe interface, resulting in lower values of local friction.

### 3.3 - Displacement-controlled cyclic loading

In order to study the local friction evolution during the application large number of cycles, it is necessary to run displacement-controlled cyclic loading sequences. The key parameters for this type of loading are the displacement amplitude (alternated or non-alternated signal), the signal shape, the frequency of the signal and the number of cycles applied. Fig. 7 presents the results corresponding to Test1, for which  $10^5$  cycles have been applied. For this typical test, the cyclic displacement amplitude  $\rho_c$  was chosen equal to  $\pm 250 \mu\text{m}$  (alternated signal) and the shape of the signal is sinusoidal (Fig. 7(a)). The cyclic displacement amplitude chosen gives a high value of  $\rho_c/\rho_{peak}$  ratio (ratio between cyclic displacement amplitude and displacement required to mobilize full friction in a static load test). The high value of this ratio allows to better highlight the effect of this parameter on the evolution of local shaft friction during cyclic loading. The test frequency chosen (1 Hz) is intended to study the case of offshore or onshore piles subjected to low speed road traffic or railway traffic (generally varying between 0.1 and 10 Hz).

A rapid degradation process is observed from the very first cycle, which keeps going for about 40 cycles (Fig. 7(b)). This degradation phase corresponds to cyclic strain-softening of the probe-soil interface. Then, a progressive recovery of mobilized friction is observed (strain-hardening) up to the end of the cyclic sequence with a slight “re-decrease” observed between cycles 300 and 900.

A coefficient of friction evolution, called  $C_{e,fs}$  (Bekki et al. (2013), Muhammed et al. (2018a)), is introduced to clearly visualize the evolution of local friction mobilization during the application of the cycles. The degradation phases corresponds to a decrease of the value of  $C_{e,fs}$  and the reinforcement phases, if there is any, corresponds to an increase of the value of this coefficient.

$$C_{e,fs} = \frac{f_{s,\max(i)} - f_{s,\min(i)}}{f_{s,\max(1)} - f_{s,\min(1)}} \quad (1)$$

where  $f_{s,\max(1)}$  and  $f_{s,\max(i)}$  are the maximum skin friction measured on first cycle and cycle  $i$  respectively (push-in phases),  $f_{s,\min(1)}$  and  $f_{s,\min(i)}$  being the values of minimum skin friction measured on first cycle and on cycle  $i$  respectively (pull-out phases).

Fig. 8 shows the evolution of  $C_{efs}$  versus number of cycles. Most of the degradation occurs within the first 40 cycles. The minimum value reached is about 0.44 which is a low value corresponding to a significant degradation level due to the large cyclic displacement amplitude selected. After the degradation phase, the reinforcement phase toward the end of the cyclic sequence can be observed with a slight decrease between cycle n° 300 to cycle n° 900. Muhammed et al. (2018a) have explained the behavior observed during the application of the cycles in terms of the evolution of the effective normal stress acting on the probe shaft,  $\sigma'_n$ . The local friction mobilized being equal to  $f_s = \sigma'_n \tan \delta_{mob}$ ,  $\delta_{mob}$  being the mobilized friction coefficient. It is well known that the evolution of effective normal stress depends on the evolution of excess pore water pressure (EPWP). Any variation of the EPWP results in a variation of effective normal stress.

Since the tested soil is a kaolinite, characterized by a rather low permeability, one can expect that the applied cyclic shear at 1 Hz frequency will result in the development of EPWP close to the soil-probe interface. A heterogeneous field of EPWP will be created within a small thickness annulus around the probe, resulting in high hydraulic gradients and initiation of EPWP dissipation. Since the interface shearing is not fully undrained, the problem is therefore coupled with combination of EPWP generation and dissipation. There is, indeed, a competition between the excess pore water pressure generation mechanism due to “undrained” cyclic deformation of the clay around the sleeve, and the EPWP dissipation, which starts taking place from the very beginning of the cyclic sequence due to the radial hydraulic gradient created by the excess pore pressure field. During the initial phase of the sequence (small numbers of cycles), the generation mechanism should be predominant with respect to dissipation, which should result in a relatively rapid increase of EPWP, a corresponding decrease in the normal effective stress and corresponding decrease of mobilized friction (cyclic strain-softening). Then, the dissipation process should become predominant, resulting in a progressive decrease of the EPWP, re-increase of  $\sigma'_n$  and corresponding re-increase of mobilized friction (cyclic strain-hardening). This hypothesis is in full agreement with the results published by Procteur and Khaffaf (1987) and Muhammed *et al.* (2018a).

### 3.4 - Final phase of static loading

The influence of the cyclic sequence on the post-cyclic static response of the interface has been investigated by performing two post-cyclic static loading tests. The two post-cyclic static tests were performed at the same displacement rate of 300  $\mu\text{m}/\text{min}$  up to failure (4 mm of vertical displacement). The first post-cyclic static test was performed directly after the end of the cyclic sequence. The second post-cyclic static test was performed after a resting period of two hours after the first test, allowing pore water pressure equilibrium of the soil around the probe. Fig. 9

shows the evolution of mobilized local friction versus vertical displacement for the two successive post-cyclic static tests. A significant difference may be observed between the two loadings tests. For the first test, a sharp peak of friction (of about 54 kPa) is obtained for a tip displacement of about 500  $\mu\text{m}$ , followed by a rapid strain softening and a stabilization at an ultimate value of about 25 kPa. For the second test, the response observed is qualitatively very similar to the response observed for the pre-cyclic static tests. No peak is observed and full mobilization of friction is obtained for a very small displacement (about 100  $\mu\text{m}$ ) followed by a constant friction plateau of about 23 kPa. It is worth noting that the ultimate value of friction obtained at large displacements is very similar for both loadings.

In order to quantify the influence of the cycles on the post-cyclic static response, the degradation factor of skin friction,  $D_\tau$  as defined by Poulos (1982), has been used:

$$D_\tau = \frac{\text{property after cyclic loading}}{\text{property for initial static loading}} \quad (2)$$

It is interesting to note that the value obtained for  $D_\tau$  factor ( $D_\tau=0.70$ ) is fairly close to the value obtained for the coefficient of evolution  $C_{e,fs}$  ( $C_{e,fs}=0.72$ ) at the end of the cyclic sequence (cycle n° 10<sup>5</sup>) accounting for a good consistency between the two coefficients.

#### 4 – INFLUENCE OF CYCLIC DISPLACEMENT AMPLITUDE AND INITIAL STATE OF SPECIMEN ON LOCAL FRICTION EVOLUTION

In order to evaluate the influence of cyclic displacement amplitude and initial state of specimen in terms of initial state of stress on the mobilization of local friction, a series of five tests has been carried out. All specimens were normally consolidated and were saturated with no application of backpressure. Table 2 summarizes the main characteristics of the tests carried out.

##### 4.1 - Influence of the cyclic displacement amplitude

A very important parameter involved in the evolution of local friction upon cyclic tests is the cyclic displacement amplitude,  $\rho_e$ , which controls the evolution of interface properties. Real piles are generally head-loaded in a force-controlled way (either monotonic or cyclic loading). However, locally, along the shaft and under cyclic loading, this head loading results, at a given depth along the pile shaft, in a cyclic displacement with a given amplitude during a certain number of cycles, controlling the interface properties evolution. The cyclic displacement amplitude is not the same at all depths along the pile shaft (usually larger toward the pile head and smaller toward the pile toe) depending on the rigidity of the pile and the head loading amplitude. The calibration chamber setup, allowing to run displacement-controlled loadings, is therefore an appropriate tool to quantify the influence of this parameter on the evolution of local interface frictional properties.

Three tests, Test 1, Test 2 and Test 3 (table 1), have been performed under the same initial state of stress applied to the specimen. These tests were intended to quantify the influence of the cyclic displacement amplitude on the evolution of mobilized local friction upon cyclic loading and subsequent post-cyclic static friction. The vertical and horizontal stresses applied to the specimen, the number of cycles and the loading frequency were kept constant while the cyclic displacement amplitude was varied from low to high values. Before presenting the behavior observed upon cyclic sequences, Fig. 10 shows the repeatability of the measurements upon pre-cyclic static tests for the three tests, indicating a good consistency between the results (with a maximum variance of 10% at failure).

The influence of the cyclic displacement amplitude on the evolution of skin friction upon cyclic loading is shown in Fig. 11 in terms of the coefficient of evolution. Three cyclic displacement amplitudes, i.e.,  $\pm 100 \mu\text{m}$ ,  $\pm 250 \mu\text{m}$  and  $\pm 500 \mu\text{m}$ , have been applied for Test 2, Test 1 and Test 3, respectively. These values of cyclic displacement amplitude represent low to high ratios of  $\rho_c/\rho_{peak}$  (ratio between cyclic displacement amplitude, applied during the cyclic sequence, and displacement required to mobilize full friction in a static load test). This Figure clearly shows that the skin friction degradation rate increases with increasing cyclic displacement amplitude. This increase of the degradation rate could be explained in terms of EPWP generation around the probe. In fact, higher values of cyclic displacement amplitude induces relatively higher values of EPWP resulting in higher decrease in the effective normal stress and corresponding higher decrease of mobilized friction (cyclic strain-softening). For high to very high values of applied cyclic displacement amplitudes, after the degradation phase, a progressive phase of reinforcement can be observed. This reinforcement phase can be attributed to the EPWP dissipation. In fact, for high values of cyclic displacement amplitude, the induced high values of EPWP around the sleeve will first increase rapidly and then decrease after passing through a maximum value due to the dissipation phenomena, which becomes predominant rapidly.

After the cyclic sequence, two post cyclic static tests has been performed for each specimen at a displacement rate of  $300 \mu\text{m}/\text{min}$  (same loading procedure as for the typical test). The influence of the cyclic displacement amplitude on the evolution of skin friction upon post-cyclic static loading is presented in Fig. 12. Qualitatively, results are similar. For the three tests, a sharp peak of skin friction is obtained upon the first post-cyclic static loading followed by significant strain softening which keeps going with progressive stabilization for large displacements. However, quantitatively, a clear distinction of the post cyclic behavior can be observed for different cyclic displacement amplitudes tested. The test results show that the peak value of skin friction, obtained upon the first post-cyclic static test, increases with increasing the cyclic displacement amplitude applied during the cyclic loading. For the lowest cyclic displacement amplitude ( $\pm 100 \mu\text{m}$ ), the corresponding peak value is 43 kPa reached at 0.25mm of probe displacement. This value of local friction is fairly close the one mobilized upon pre-cyclic static tests while for the highest cyclic displacement amplitude ( $\pm 500 \mu\text{m}$ ), the corresponding peak value is 70 kPa reached after 0.95mm of probe displacement. It is interesting to note that the required displacement to reach the full mobilization of local friction (peak of local friction), upon post-cyclic static tests, also increases with increasing the cyclic displacement amplitude (Fig. 13).

One may attribute the variation in the values of the peak and required displacement to reach the peak, to the induced thickness of the modified zone around the probe after cyclic loading. The authors believe that higher cyclic displacement amplitude influences larger zone within the soil around the probe, thus resulting in a thicker modified interface zone. The soil within this zone, characterized as the modified zone of interface, undergoes shearing and variation of EPWP during the cyclic loading (coupled generation and dissipation phases). Recently, Muhammed *et al.* (2019) showed that the soil within this zone presents a very different type of response upon post-cyclic static tests with respect to the one observed for the initial pre-cyclic static loadings. These authors have observed a significant decrease of the measured PWP (generation of negative excess pore water pressure EPWP) at the clay-probe interface upon post-cyclic static tests accounting for the modification of the soil-probe interface properties after cyclic loading. The authors have also indicated that this negative EPWP corresponds to a dilative behavior representative of an overconsolidated state of the clay at the soil-probe interface due to the cyclic loading. Thus, after the cyclic loading, the thicker overconsolidated modified zone around the probe presents higher values of friction and requires necessarily more displacement to be sheared upon post-cyclic static test, as shown on the 2D conceptual scheme presented in Fig. 14.

In terms of friction degradation at the end of each loading stage, i.e. end of cyclic and post-cyclic static loadings, results show close values between the coefficient of evolution,  $C_{e,fs}$ , at the end of cyclic loading and degradation factor of skin friction obtained from static tests,  $D_\tau$ , which is consistent and gives more confidence to the results obtained.

## 4.2 - Influence of the initial state of effective stress applied to the specimen

Another parameter that can be investigated in calibration chamber is initial state of effective stress applied to the specimen. This parameter is representative of a given depth within the soil below the ground surface: the higher the effective state of stress and the deeper the soil element. In calibration chamber, the effect of this parameter can be investigated by changing the values of horizontal and vertical confining pressure applied to the specimen. This allows to study the behavior of a pile segment at any depth.

Results of three tests, Test 1, Test 4 and Test 5 (Table 1), with three different initial states of stress, have been compared, corresponding to the state of a pile segment at three different depths below the ground surface.

The same loading procedure as the one described in the typical test was implemented here again for successive loading sequences: installation phase, pre-cyclic static phases, cyclic sequence and for post-cyclic static phases. The influence of the initial state of effective stress on the evolution of local friction versus probe penetration during the installation and subsequent pre-cyclic static tests is presented in Fig. 15. For the three stress levels tested, the mobilized skin friction and initial stiffness increase linearly with increasing the applied effective state of stress, which is consistent. It is important to notice that, upon initial static tests, the required displacement to mobilize full local friction increases with increasing the effective consolidation stress level.

The influence of the initial state of stress on the evolution of skin friction upon cyclic loading is shown in Fig. 16. The cyclic displacement amplitude, the number of cycles and the loading frequency were the same for the three tests. Again, the comparison is made in terms of coefficient of evolution. This figure shows that the rate of local friction degradation decreases with the increase in the initial effective stress. This can be explained in terms of the  $\rho_c/\rho_{peak}$  ratio, which dominates the amount of degradation of the interface (Poulos (1982)). The higher the value of  $\rho_c/\rho_{peak}$  ratio and the higher the degradation rate. For the three cyclic tests presented here, the  $\rho_{peak}$  value increases with increasing initial effective state of stress (visible in Fig. 15b) resulting in lower values of  $\rho_c/\rho_{peak}$  ratio and corresponding smaller rates of friction degradation.

As far as the post-cyclic static responses are concerned, results show that the mobilized local friction (maximum value  $f_{s,peak}$  and ultimate value  $f_{s,lim}$ ) increases with increasing initial effective state of stress. However, the required displacement to mobilize full local friction after the cyclic sequence decreases with increasing initial effective state of stress. This could be explained, again, in term of thickness of the modified zone created after cyclic loading. Since upon cyclic loading, higher initial effective state of stress allows lower degradation. It is thus believed that, thinner modified interface zone is formed for higher levels of applied effective stress after the cyclic loading. This means that the modified interface zone created for low consolidation stress level ( $\sigma'_{v0} = 125$  kPa -  $\sigma'_{h0} = 72$  kPa) is thicker than the ones formed for medium ( $\sigma'_{v0} = 250$  kPa -  $\sigma'_{h0} = 150$  kPa) and high ( $\sigma'_{v0} = 420$  kPa -  $\sigma'_{h0} = 252$  kPa) consolidation stress level, requiring necessarily more displacement to be sheared upon post-cyclic static test. It is also instructive to estimate the degradation factor of skin friction from Fig. 17. The specimen with the higher initial state of stress corresponds to higher  $D_\tau$  factor value corresponding to lower amount of degradation. The estimated values of  $D_\tau$  factor are 0.58, 0.70 and 0.88 for ( $\sigma'_{v0} = 125$  kPa -  $\sigma'_{h0} = 72$  kPa), ( $\sigma'_{v0} = 250$  kPa -  $\sigma'_{h0} = 150$  kPa) and ( $\sigma'_{v0} = 420$  kPa -  $\sigma'_{h0} = 252$  kPa) respectively. It is interesting to note that there is a reasonable agreement between the degradation factor values and the coefficient of evolution values at the end of cyclic loading.

## 5 –SYNTHESIS OF THE RESULTS

To better analyze the effect of cyclic displacement amplitude and initial state of stress applied to the specimen, on the local interface friction, the results of the present work are synthesized in this section. Concerning the local friction mobilization upon displacement-controlled static tests, Fig. 18 shows the evolution of maximum and ultimate values reached in terms of local friction upon static tests. In the same figure, a comparison is made with the maximum value of friction mobilized upon installation phase. Results clearly show a quasi-linear relationship between the local friction and initial state of effective stress (Fig. 18a and 18b). The higher the initial state of effective stress and the higher the values of mobilized local friction. Fig. 18a and 18b also emphasize that the mobilized local friction upon installation phase is much smaller than the one mobilized upon initial static loadings (nearly half). This aspect has been explained by the fact that during installation phase, high local values of excess pore water pressure is

generated due to the high increase of total stresses during the deep penetration process as the soil is forced outwards to accommodate the volume of the probe. This, decreases the effective normal stress acting on the pile shaft and by consequent, the mobilized friction reduces. During static loadings, the applied displacement rate is significantly smaller and the corresponding EPWP generation within the soil is limited to a thin layer around the probe. The corresponding mobilization is then higher. This interpretation is in reasonable agreement with the results published by Randolph (2003), Gavin and Gallagher (2005), O'Beirne (2016) and Hosseini and Rayhani (2017) and Muhammed *et al.* (2019).

As far as the effect of cyclic loading parameters on the evolution of local friction is concerned, in Fig. 19, the relationship between the coefficient of evolution and the degradation factor with the applied cyclic displacement amplitude and the initial consolidation level is synthetized.

This figure has an important practical implication as it demonstrates clearly the effect of both parameters on the degradation of local skin friction. Fig. 19a synthetizes the effect of cyclic displacement amplitude on the evolution of the degradation factor and of the coefficient of evolution. The figure shows clearly that the minimum value of  $C_{e,fs}$ , corresponding to maximum degradation, decreases with the increase in the applied cyclic displacement amplitude, which is consistent and has been explained in terms of EPWP generation around the probe. The values of  $C_{e,fs}$  at the end of the cyclic tests, i.e. cycle number  $10^5$ , are fairly close for the three cyclic displacement amplitudes after converging towards a completely drained regime with full dissipation of EPWP and corresponding re-increase of effective normal stress. The values of  $C_{e,fs}$  at the end of the cyclic tests are confirmed by the values of degradation factor  $D_\tau$ .

Fig. 19b synthetizes the effect of initial state of effective stress on the evolution of the degradation factor and the coefficient of evolution. This figure shows clearly that the minimum value of  $C_{e,fs}$ , corresponding to maximum degradation, increases with the increase in effective horizontal stress. This aspect has been explained in terms of the thickness of the influenced zone created by the cyclic loading, which should be smaller for higher effective horizontal stress. The values of  $C_{e,fs}$  at the end of the cyclic tests, i.e. cycle number  $10^5$ , and  $D_\tau$  also increase with the increase of effective horizontal stress thus confirming the above interpretations made. Finally, Table 3 gives a brief synthesis of the results in terms of the coefficient of evolution and degradation factor. A reasonable degree of consistency in the results can be observed.

## 6 – CONCLUSIONS

Evolution of local friction mobilisation during static and cyclic axial loadings at various initial state of stress and at different cyclic displacement amplitude was investigated. The experiment is based on the use of an instrumented pile-probe installed and loaded in specimens of saturated clay reconstituted in a calibration chamber. The following conclusions can be drawn:

- The local friction mobilized upon installation phase is much smaller than the one mobilized upon initial static loadings.
- The local friction and displacement required to mobilize full friction in a static test increase with increasing the initial state of effective stress applied to the specimen.



- The cyclic degradation of local friction is mainly controlled by the cyclic displacement amplitude applied. For the same initial state of the specimen, number of cycles and cyclic frequency, the skin friction degradation is higher for higher values of cyclic displacement amplitude.
- The cyclic displacement amplitude causing major friction degradation can be directly related to the displacement required to mobilize full local friction in a static test.
- For the same cyclic displacement amplitude, number of cycles and frequency, the skin friction degradation is smaller for higher values of initial consolidation pressure.

## REFERENCES

Al-Douri R H, Poulos H G (1995) Predicted and Observed Cyclic Performance of Piles in calcareous sand. *Journal of Geotechnical Engineering, ASCE*, 121 (1): 1-16.

Bekki H, Canou J, Tali B, Dupla J-C, Bouafia A (2013) Evolution of Local Friction Along a Model Pile Shaft in a Calibration Chamber for a Large Number of Loading Cycles. *Comptes Rendus – Mécanique*, 341(6): 499-507.

Chan S F, Hanna T H (1980) Repeated Loading on Single Piles in Sand. *Journal of Geotechnical and Geoenvironmental Engineering, ASCE*, 106(2): 171-188.

Chin J T, Poulos H G (1996) Tests on Model Jacked Piles in Calcareous Sand. *Geotechnical Testing Journal*, 19(2): 164-180. <https://doi.org/10.1520/gtj10339j>

Gavin K, Gallagher D (2005) Development of Shaft Friction on Driven Piles in Sand and Clay. Paper Presented to Engineers Ireland, 10th October 2005. Available at <https://www.semanticscholar.org/paper/Development-of-Shaft-Friction-on-Driven-Piles-in-Gavin-Gallagher/957b91160966903d760be8eb31deb693e0e36eab>

Goulois A, Whitman RV, Høeg K (1985) Effects of Sustained Shear Stresses on the Cyclic Degradation of Clay. In STP883-EB *Strength Testing of Marine Sediments: Laboratory and*

In-Situ Measurements, ed. R. Chaney and K. Demars, (pp. 336-351). West Conshohocken, PA: ASTM International, 1985. doi: <https://doi.org/10.1520/STP36344S>

Hosseini M A, Rayhani M (2017) Evolution of pile shaft capacity over time in marine soils. International Journal of Geo-Engineering, 8(1), 12. <http://doi.org/10.1186/s40703-017-0049-8>

Le Kouby A, Canou J, Dupla J-C (2004) Behaviour of Model Piles Subjected to Cyclic Axial Loading. Cyclic Behaviour of Soils and Liquefaction Phenomena, pp.159–166.

Lee C Y, Poulos H G (1990) Experimental Investigation of Axial Capacity of Model Grouted Piles in Marine Calcareous Sediments. Research Report No. R618, University of Sydney, School of Civil and Mining Engineering.

Lee C Y, Poulos H G (1993) Cyclic analysis of axially loaded piles in calcareous soils. Canadian Geotechnical Journal, 1993, 30(1): 82-95, <https://doi.org/10.1139/t93-008>

Lehane B M, White D J (2004) Friction Fatigue on Displacement Piles in Sand. Géotechnique, 54(10): 645-658. <https://doi.org/10.1680/geot.2004.54.10.645>

Matlock H, Bogard D, Cheang L (1982) A Laboratory Study of Axially Loaded Piles and Pile Groups Including Pore Pressure Measurements. In Proceeding of The Third International Conference on the Behavior of Offshore Structure (BOSS), Vol. 1, pp 105-121.

Mochtar I B, Edil T B (1988) Shaft resistance of model pile in clay. Journal of Geotechnical Engineering, 114(11): 1227-1244. [https://doi.org/10.1061/\(ASCE\)0733-9410\(1988\)114:11\(1227\)](https://doi.org/10.1061/(ASCE)0733-9410(1988)114:11(1227))

Muhammed R D (2015) Etude en Chambre d'étalonnage du Frottement Sol-Pieu sous  
 Grands Nombres de Cycles. Application au Calcul des Fondations Profondes dans les Sols  
 Fins Saturés. Doctoral thesis. Université Pierre et Marie Curie - Paris VI, 219 p. Available  
 at <https://tel.archives-ouvertes.fr/tel-01335671>

Muhammed R D, Canou J, Dupla J-C, Tabbagh A (2018 a) Evaluation of local soil-pile  
 friction in saturated clays under cyclic loading. Soils and Foundations 58, no. 6 (December  
 2018): 1299–1312. <https://doi.org/10.1016/j.sandf.2018.06.006>

Muhammed R D, Canou J, Dupla J-C, Tabbagh A (2018 b) Laboratory Study of Local Clay-  
 Pile Friction Evolution for Large Numbers of Cycles. In: Tran-Nguyen HH., Wong H.,  
 Ragueneau F., Ha-Minh C. (eds) Proceedings of the 4th Congrès International de  
 Géotechnique - Ouvrages -Structures. CIGOS 2017. Lecture Notes in Civil Engineering,  
 vol 8. Springer, Singapore, [https://doi.org/10.1007/978-981-10-6713-6\\_74](https://doi.org/10.1007/978-981-10-6713-6_74)

Muhammed R D, Canou J, Dupla J-C, Tabbagh A (2019) Evaluation of local friction and  
 pore water pressure evolution along instrumented probes in saturated clay for large numbers  
 of cycles. Canadian Geotechnical Journal. <https://doi.org/10.1139/cgj-2017-0408>

O'Beirne C P (2016) Development of design approaches for dynamically installed anchors  
 validated through field and centrifuge studies. Doctoral Thesis, The University of Western  
 Australia.

Poulos H G (1981) Some Aspects of Skin Friction of Piles in Clay Under Cyclic Loading.  
 Geotechnical Engineering, ASCE, 12: 1-17

Poulos H G (1982) Influence of Cyclic Loading on Axial Pile Response. R413 Monograph, University of Sydney, Sydney, New South Wales 2006 Australia, 22 p. available at <https://vulcanhammerinfo.files.wordpress.com/2017/08/poulos.pdf>

Procter D C, Khaffaf J H (1987) Cyclic axial displacement tests on model piles in clay. Géotechnique 37(4): 505-509. <https://doi.org/10.1680/geot.1987.37.4.505>

Randolph M F (2003) Science and empiricism in pile foundation design. Geotechnique, 53(10), pp 847–875. <https://doi.org/10.1680/geot.2003.53.10.847>

Tsuha C H C, Foray P Y, Jardine R J, Yang Z X, Silva M, Rimoy S (2012) Behaviour of Displacement Piles in Sand Under Cyclic Axial Loading. Soils and Foundations, 52(3): 393-410. <https://doi.org/10.1016/j.sandf.2012.05.002>

## A parametric study on the evolution of cyclic clay-pile interface friction for large numbers of cycles

### Figures

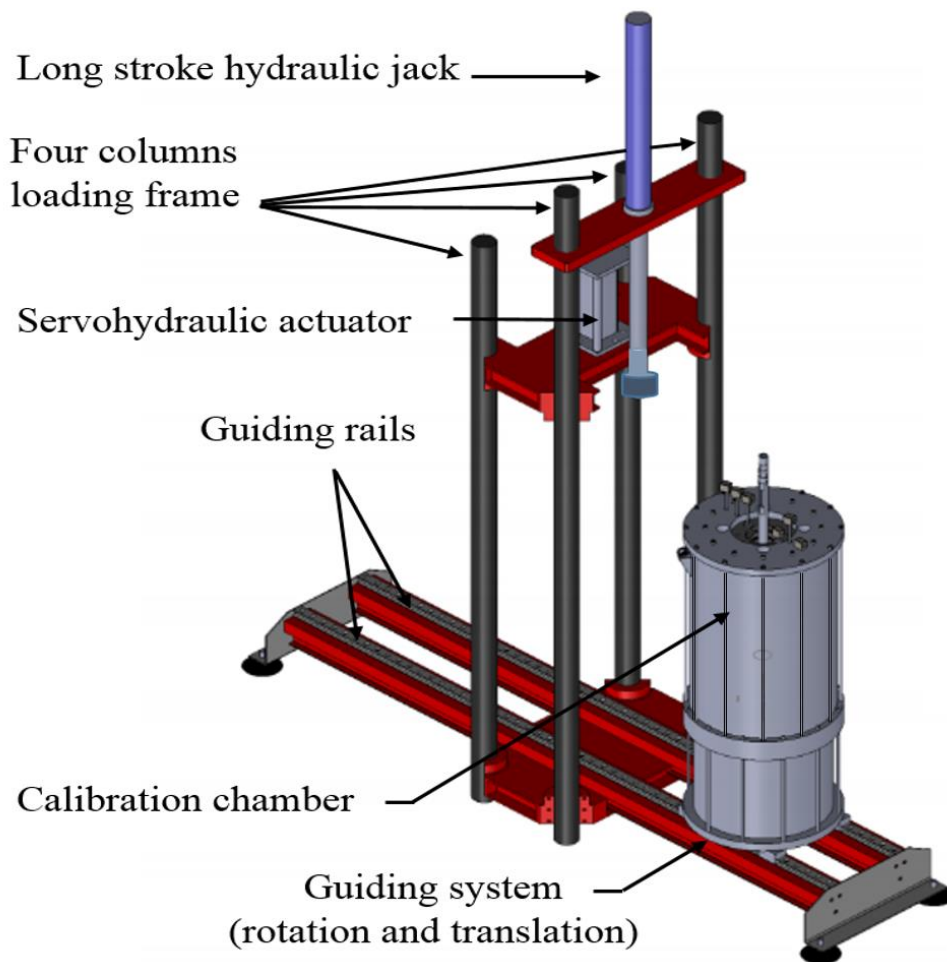


Fig. 1. General 3D view of the experimental setup

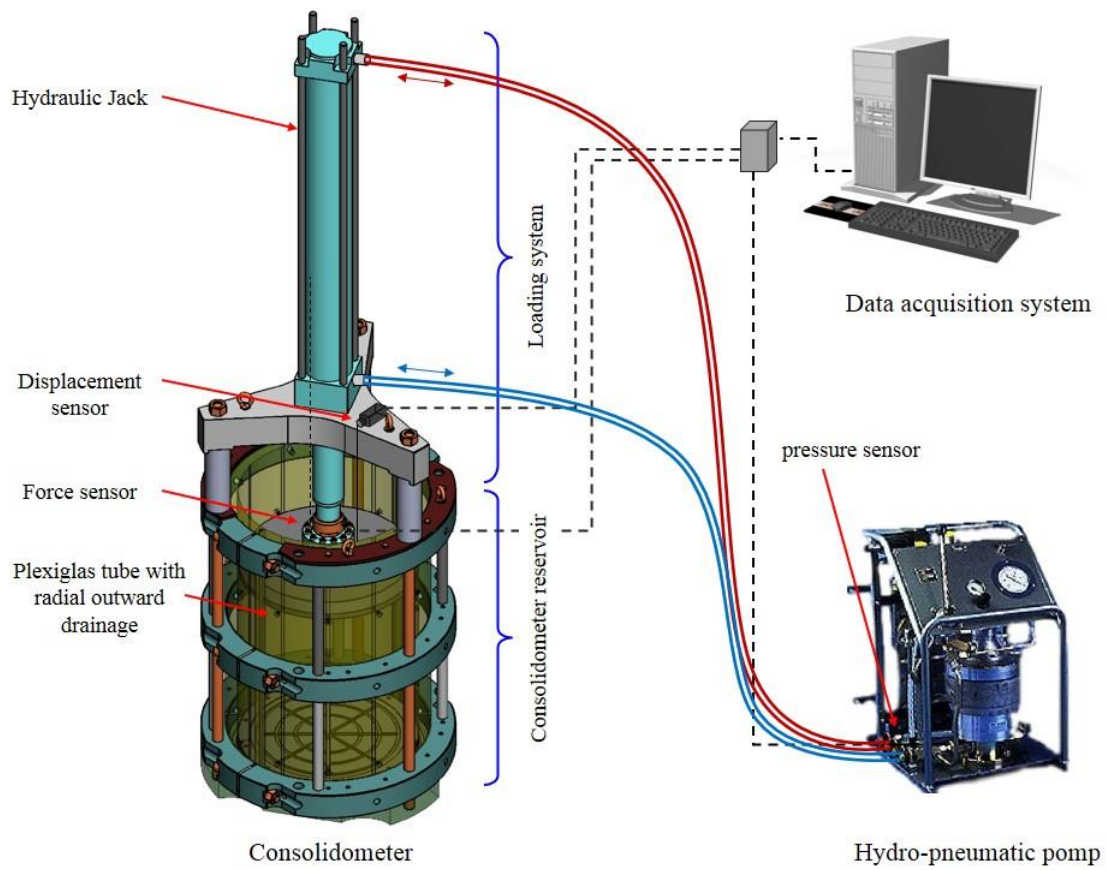


Fig. 2. General view of the consolidometer set up and ancillary equipment

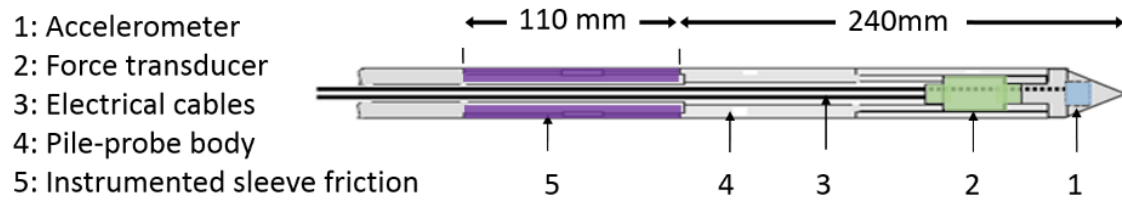


Fig. 3. Simplified cross-section and view of the instrumented pile-probe

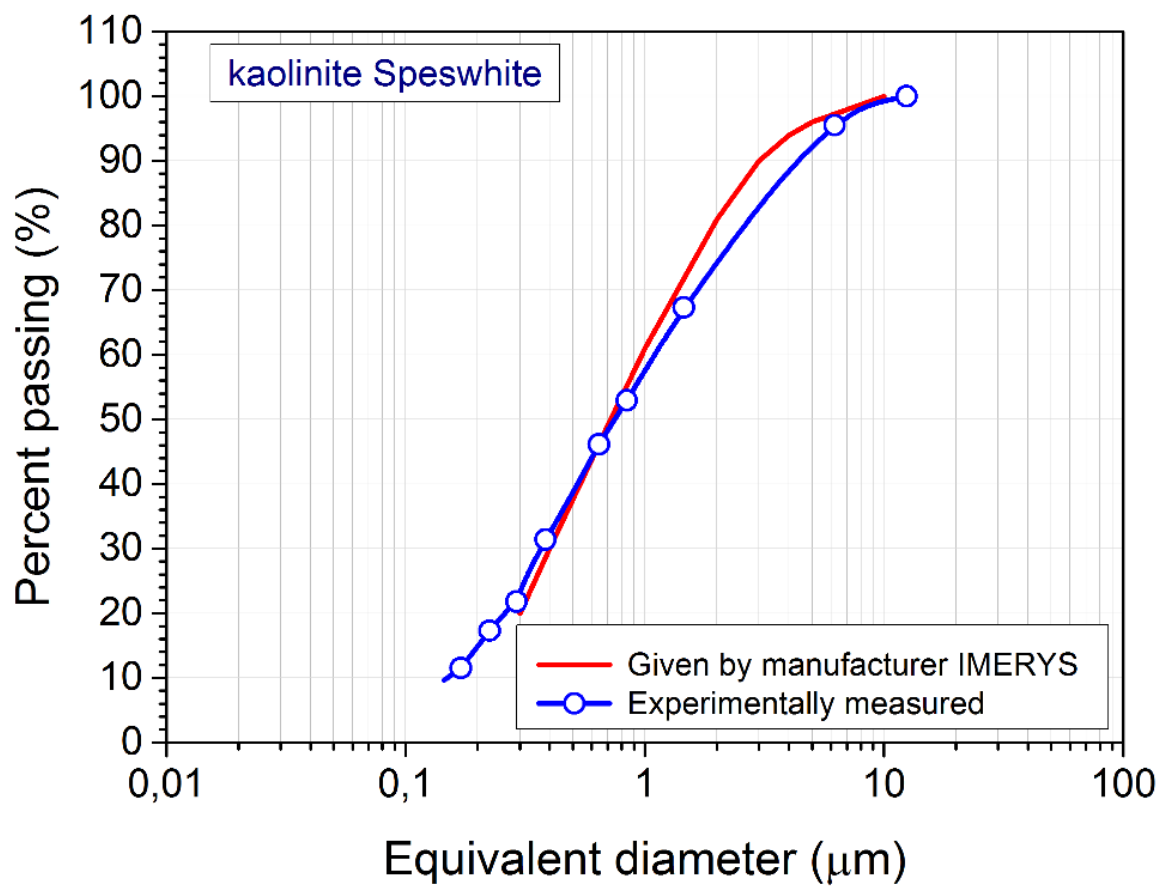


Fig. 4. Particle size distribution of Speswhite



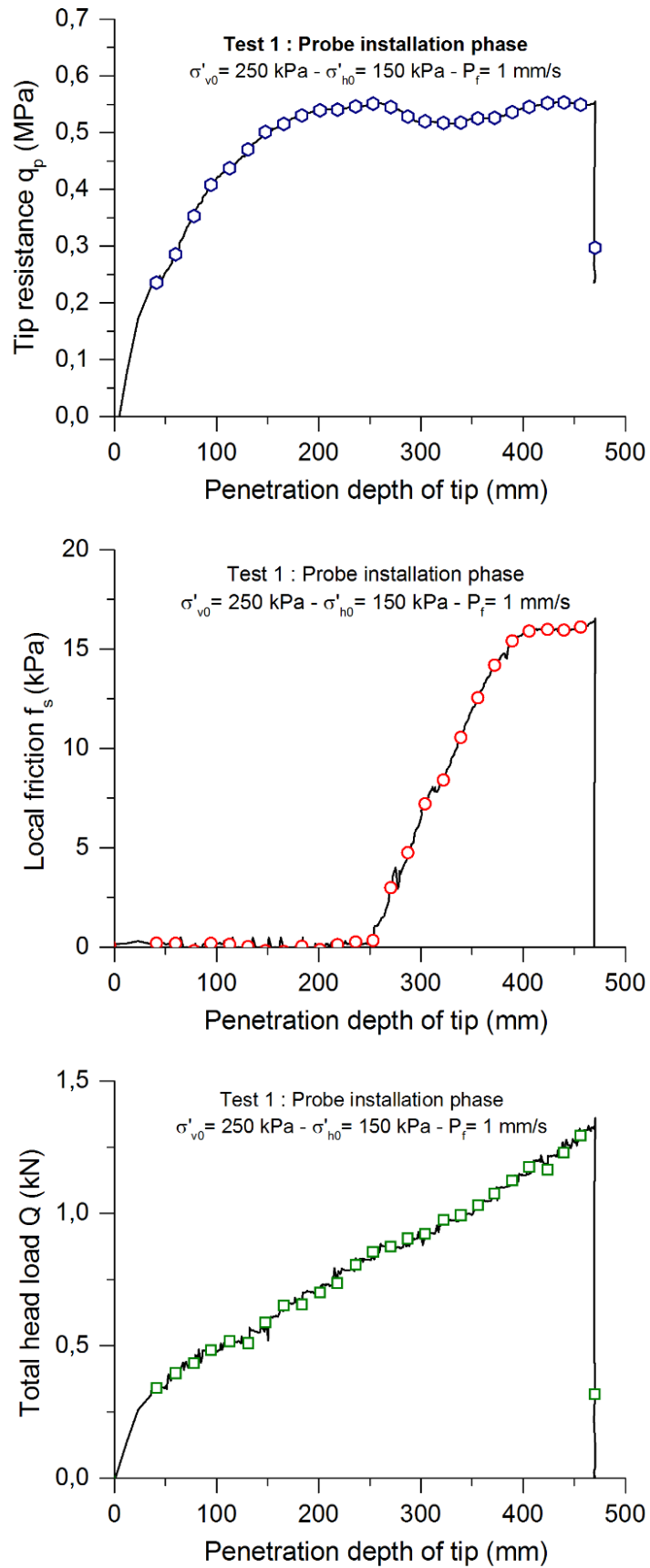


Fig. 5. Installation phase: (a) tip resistance versus penetration depth; (b) local friction versus penetration depth; (c) total load applied versus penetration depth

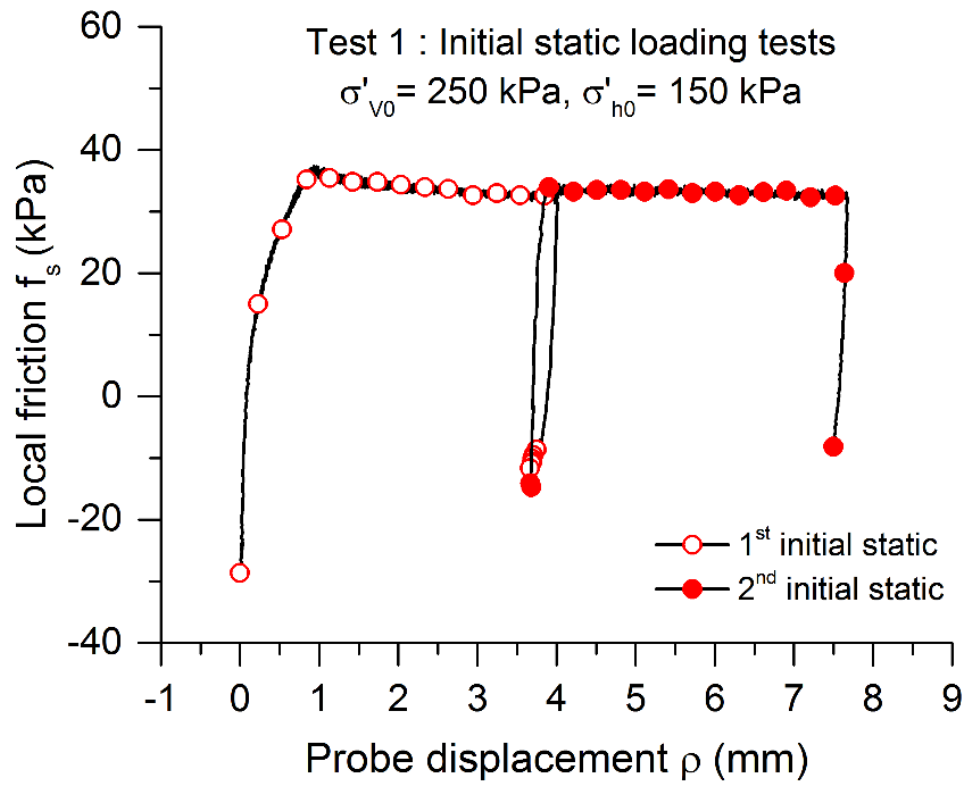


Fig. 6. Initial static loading tests: (a) tip resistance versus vertical displacement; (b) local friction versus vertical displacement; (c) total load applied versus vertical displacement

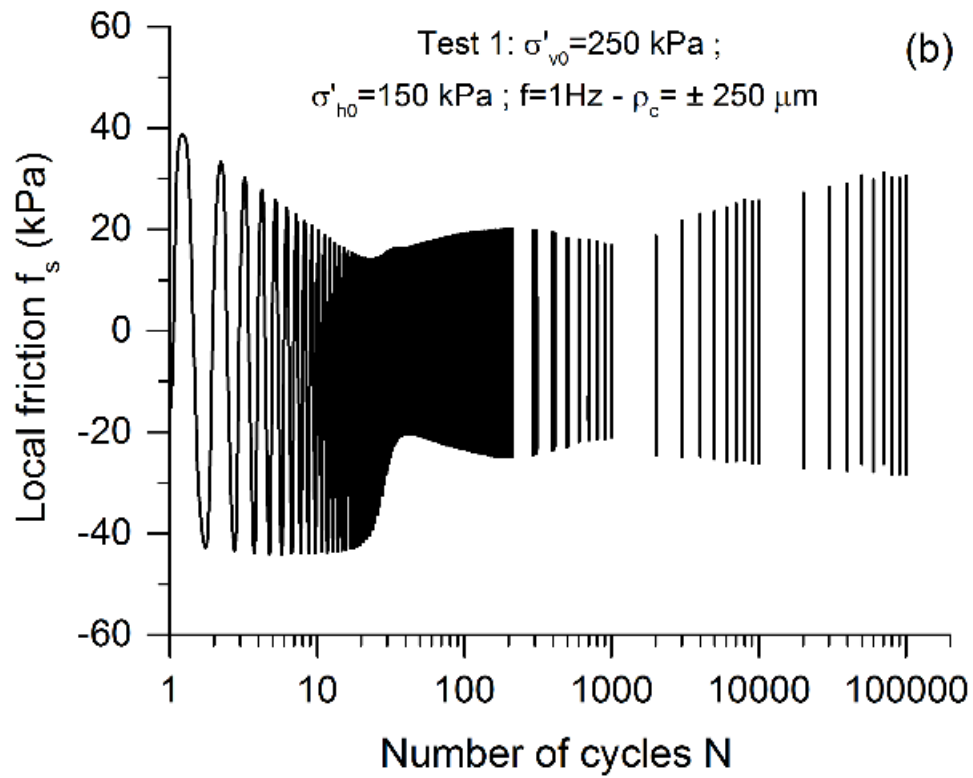
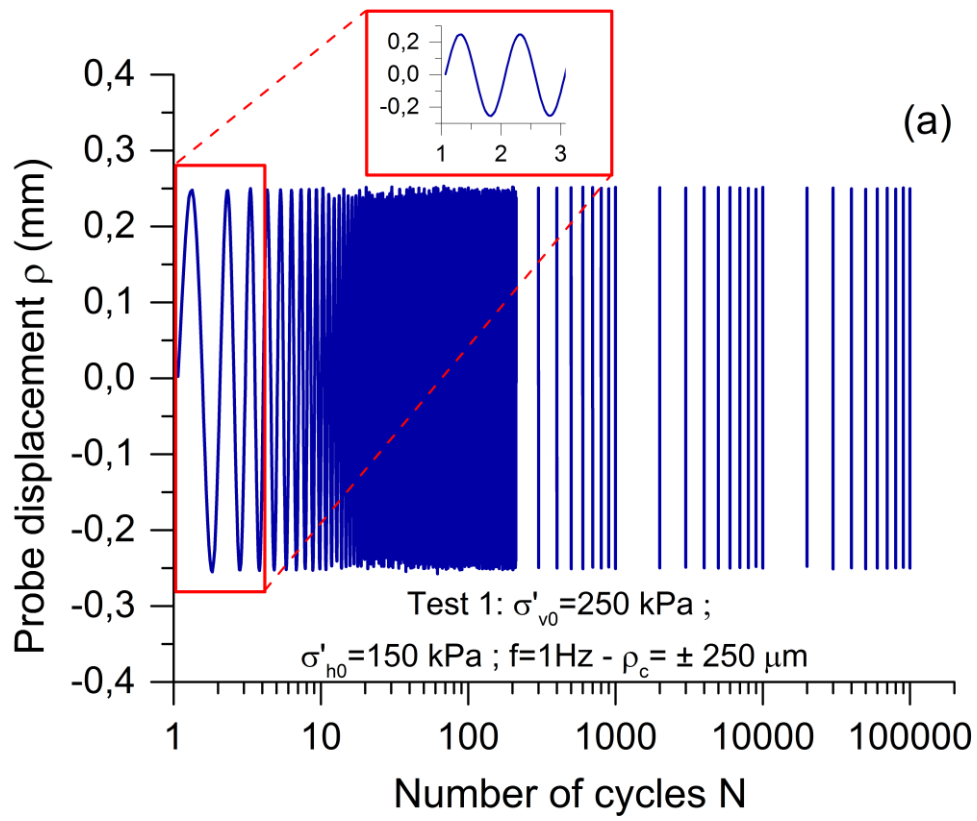


Fig. 7. Cyclic loading phase: (a) displacement-controlled loading signal versus number of cycles;  
 (b) local friction versus number of cycles

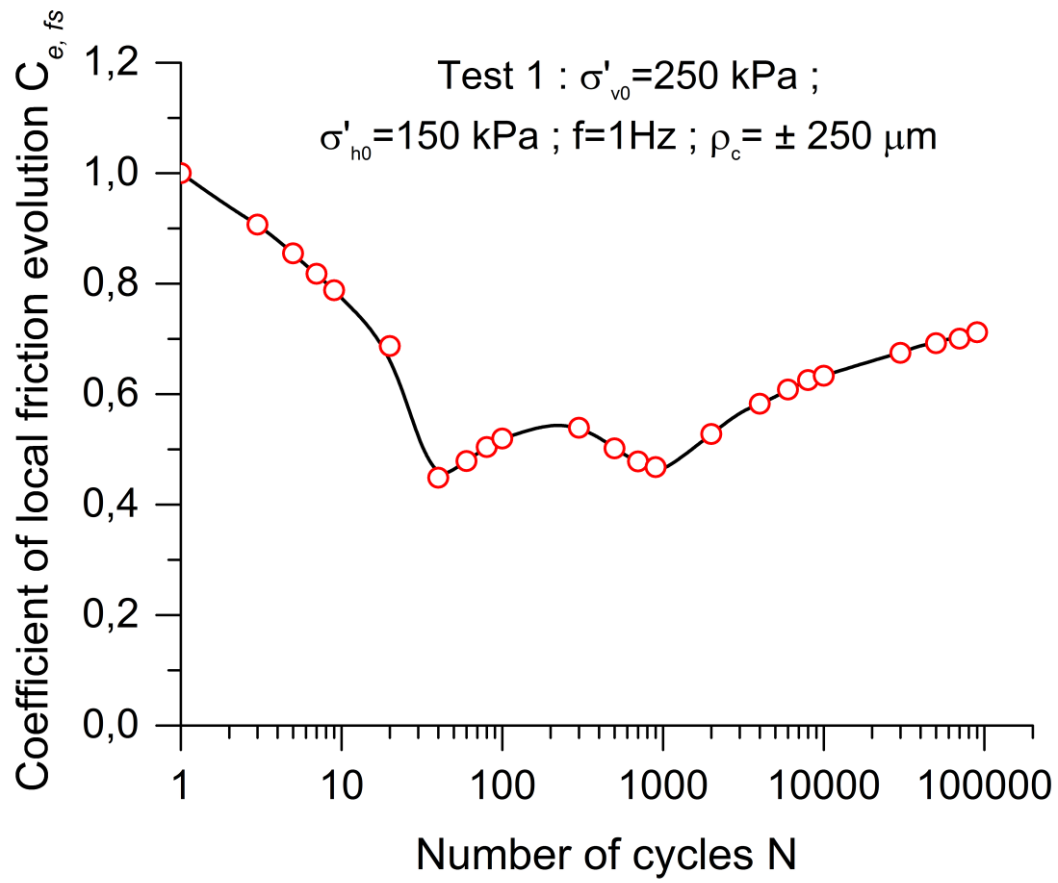


Fig. 8. Cyclic sequence: Coefficient of evolution ( $C_{e,fs}$ ) versus number of cycles

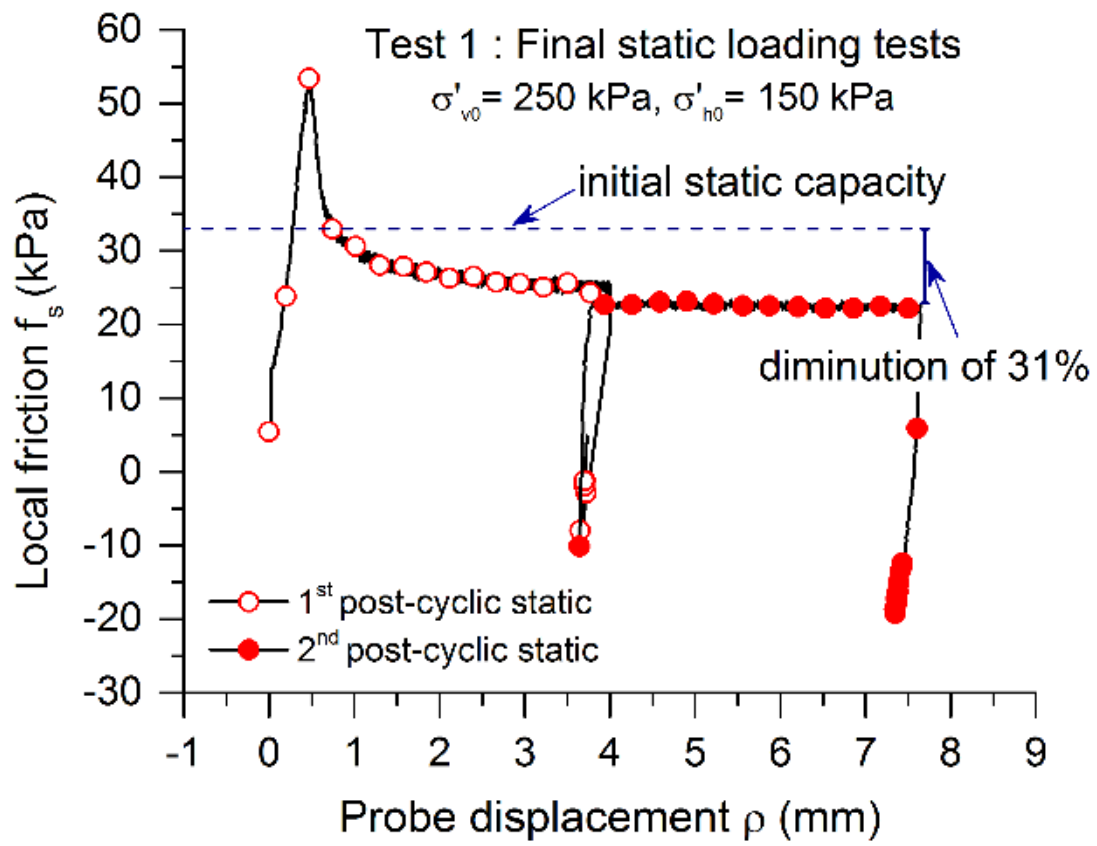


Fig. 9. Final static loading phase: (a) tip resistance versus vertical displacement; (b) local friction versus vertical displacement

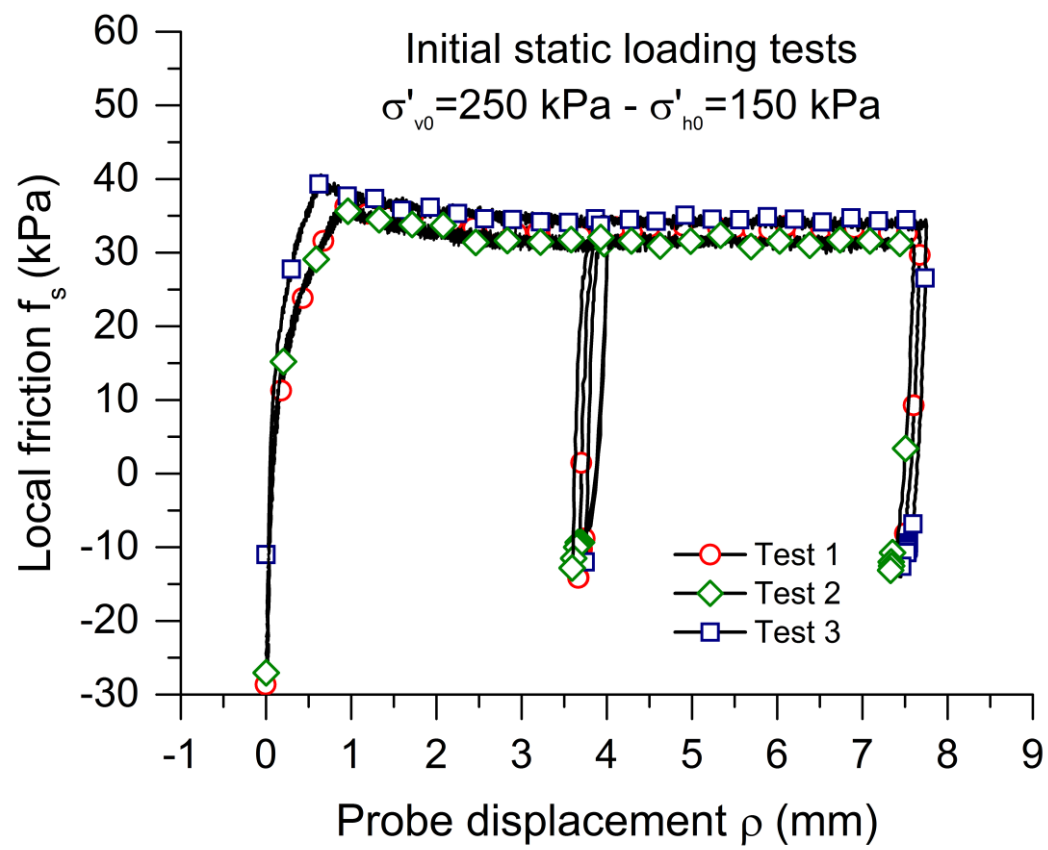


Fig. 10. Repeatability of pre-cyclic static tests

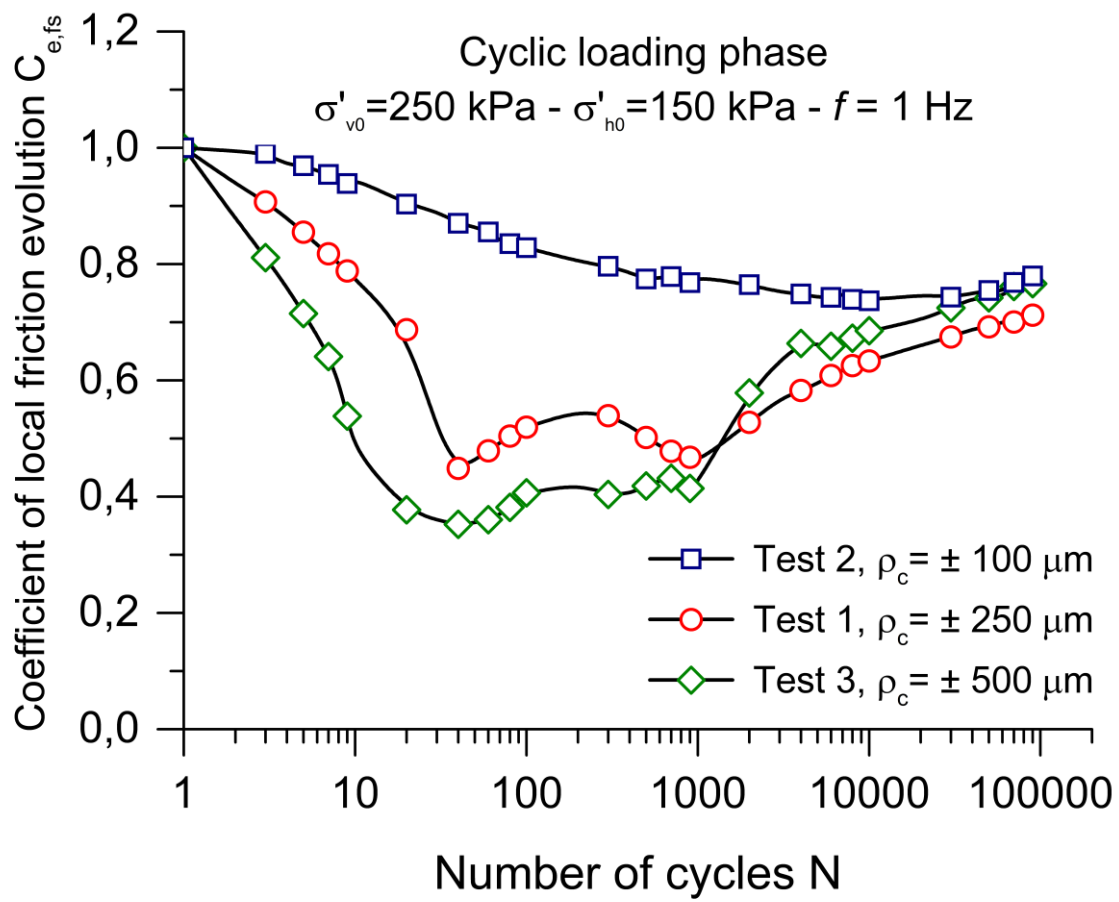


Fig. 11. Influence of the cyclic displacement amplitude on the evolution of local friction upon cyclic loading

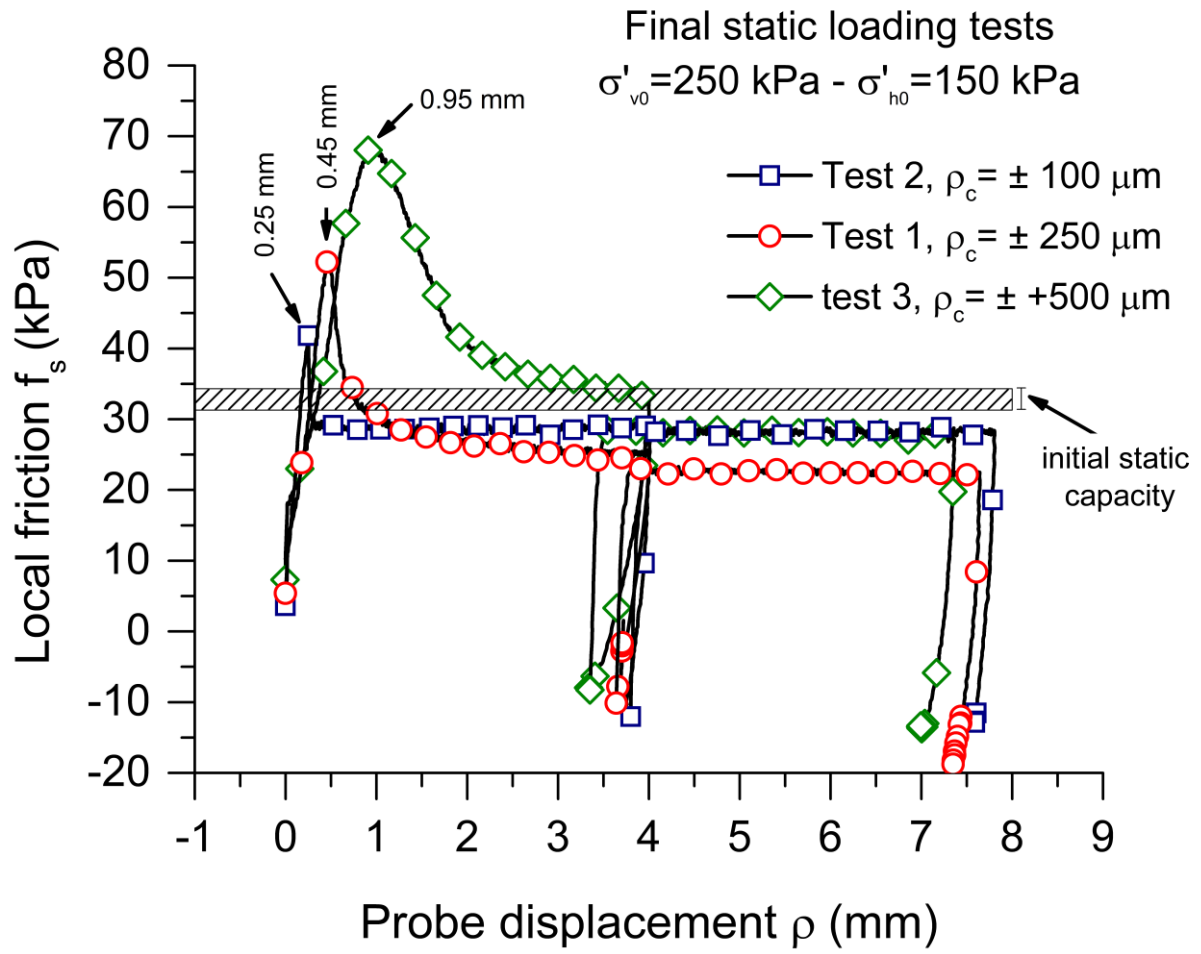


Fig. 12. Influence of cyclic displacement amplitude on the evolution of local friction upon post-cyclic static loadings



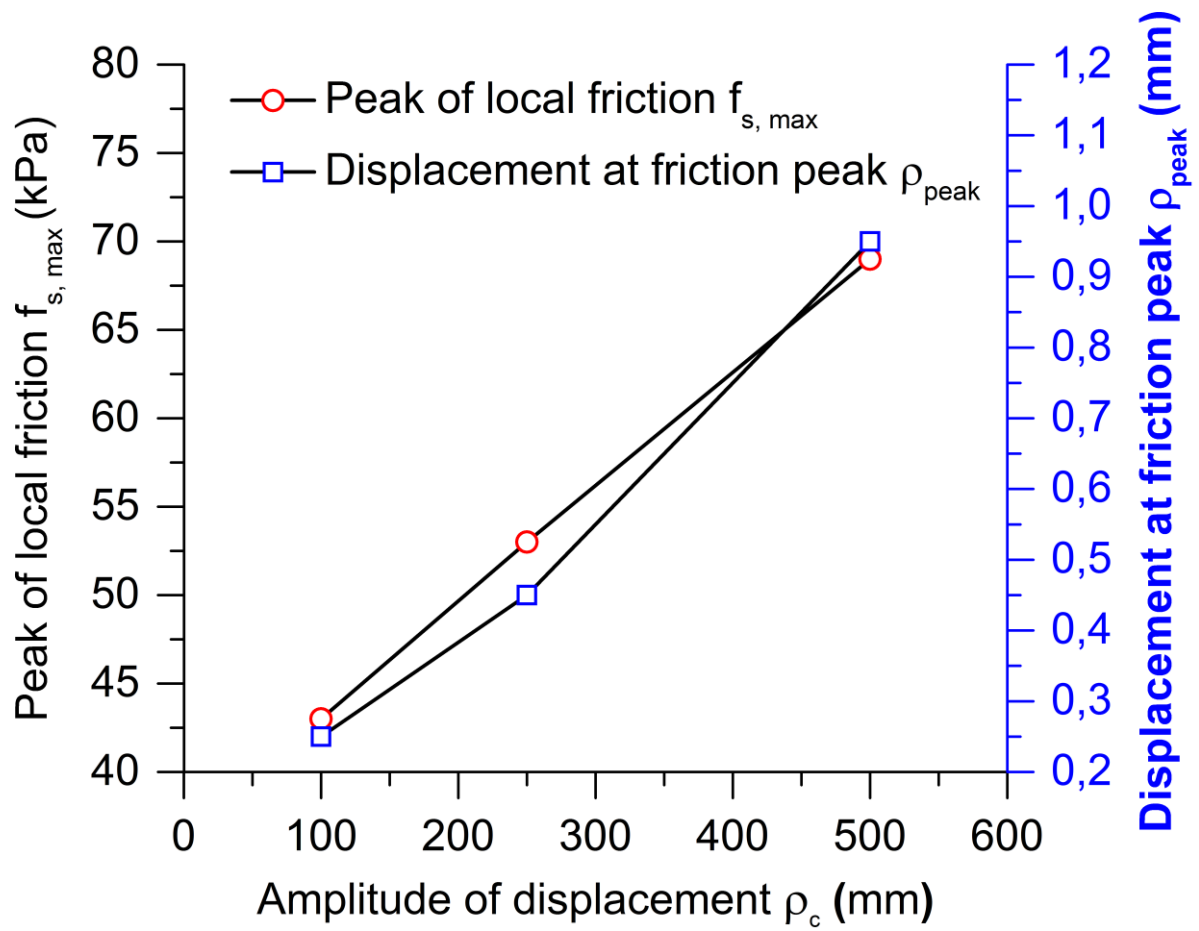
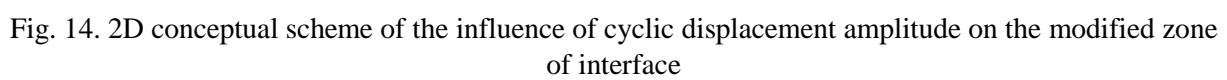


Fig. 13. Influence of cyclic displacement amplitude on the peak of local friction and the necessary displacement to reach the peak upon post-cyclic static loading



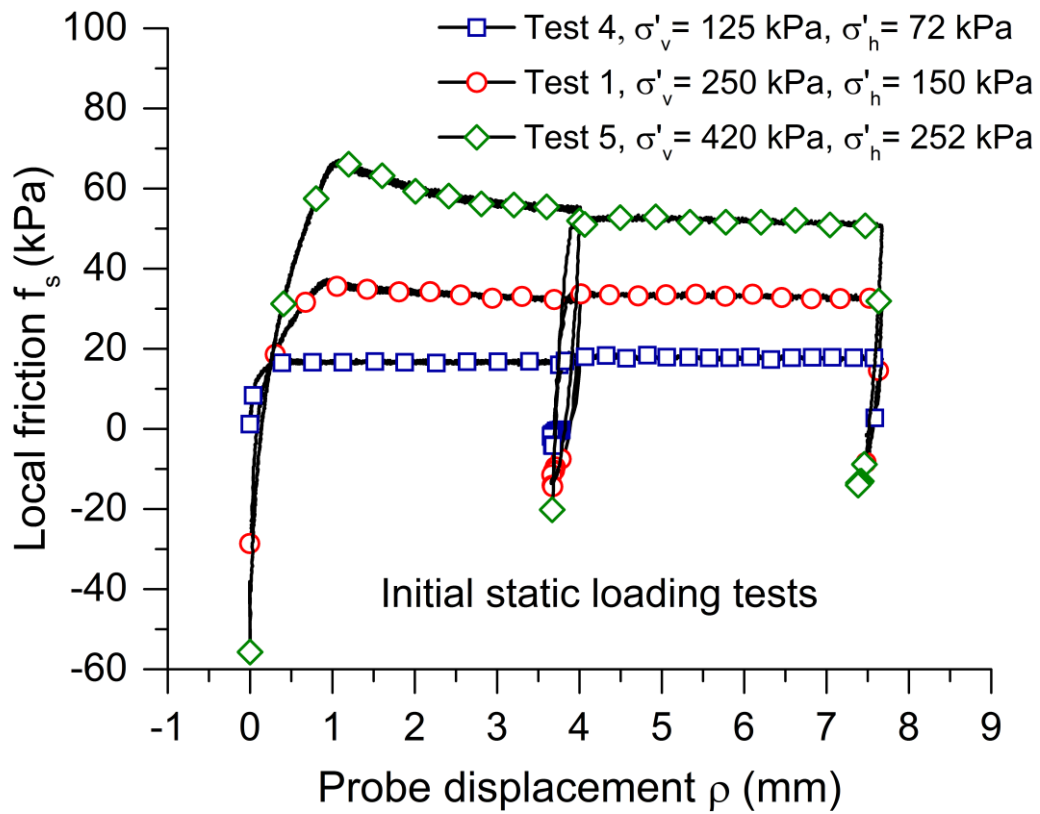
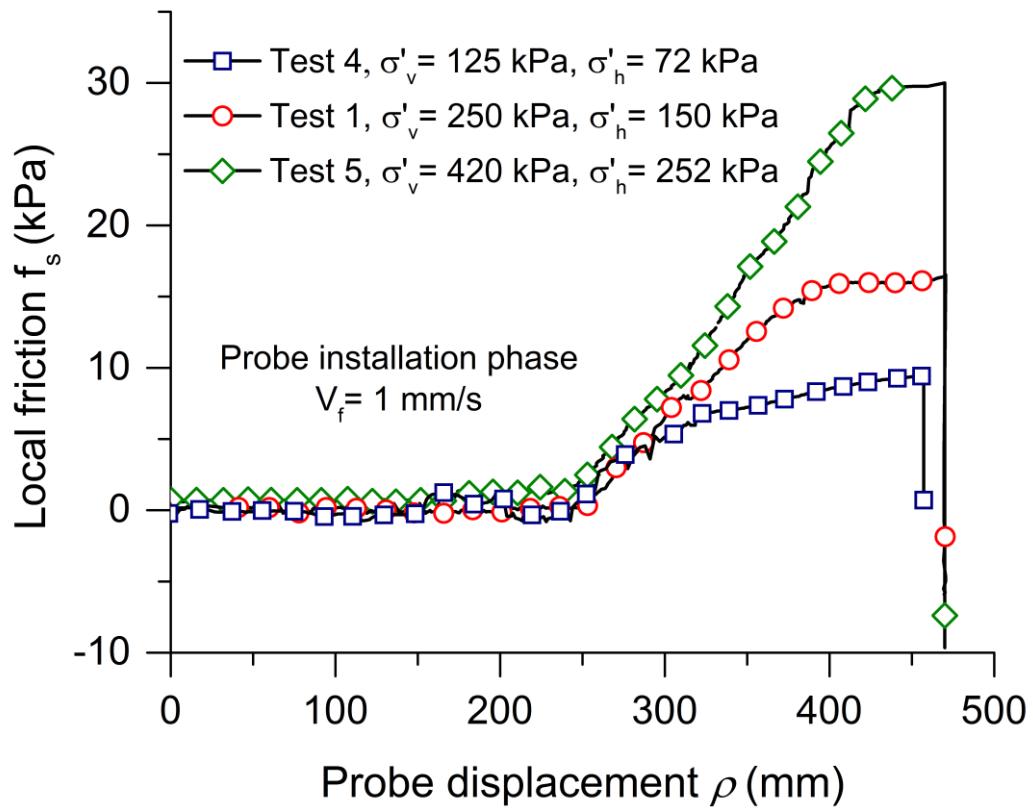


Fig. 15. Influence of initial effective consolidation stress level on the evolution of local friction upon installation and pre-cyclic static loading phases

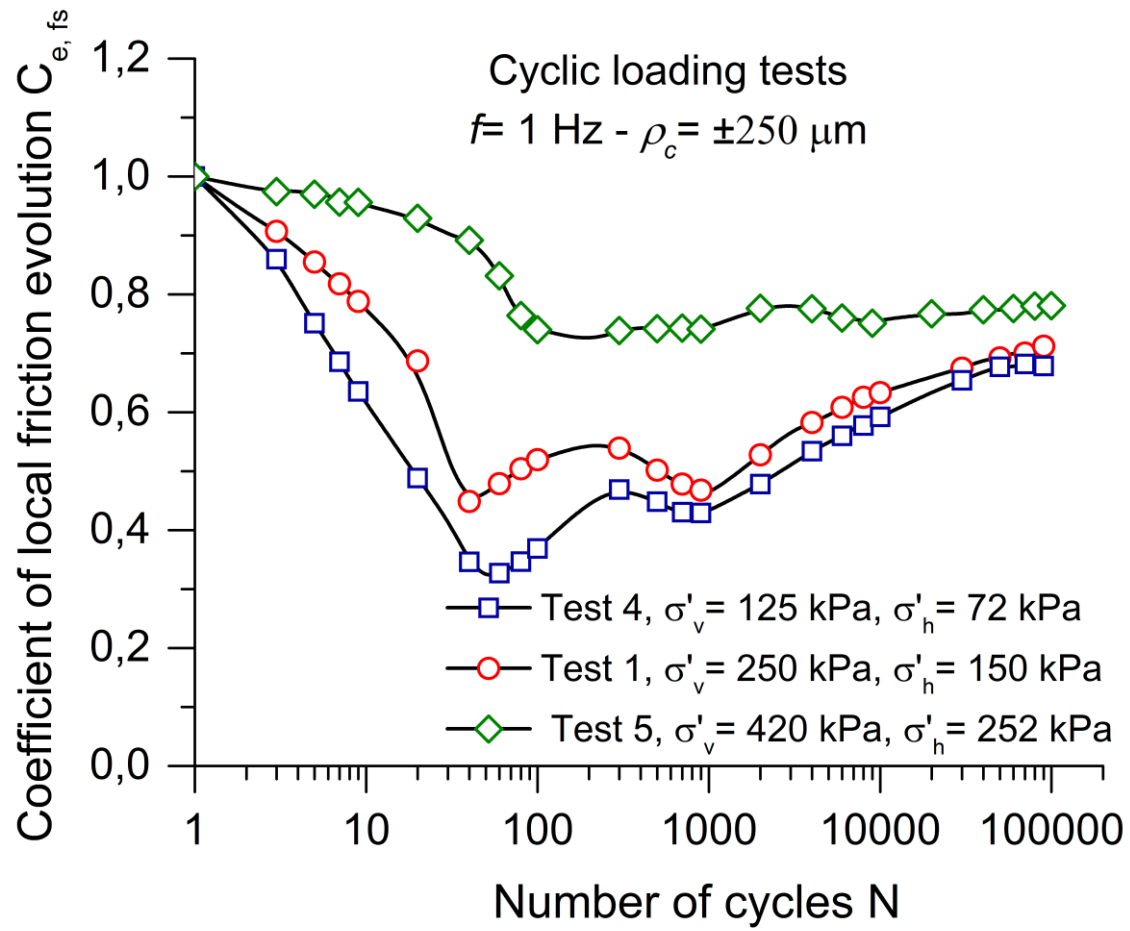


Fig. 16. Influence of initial effective consolidation stress level on the evolution of local friction upon cyclic loading

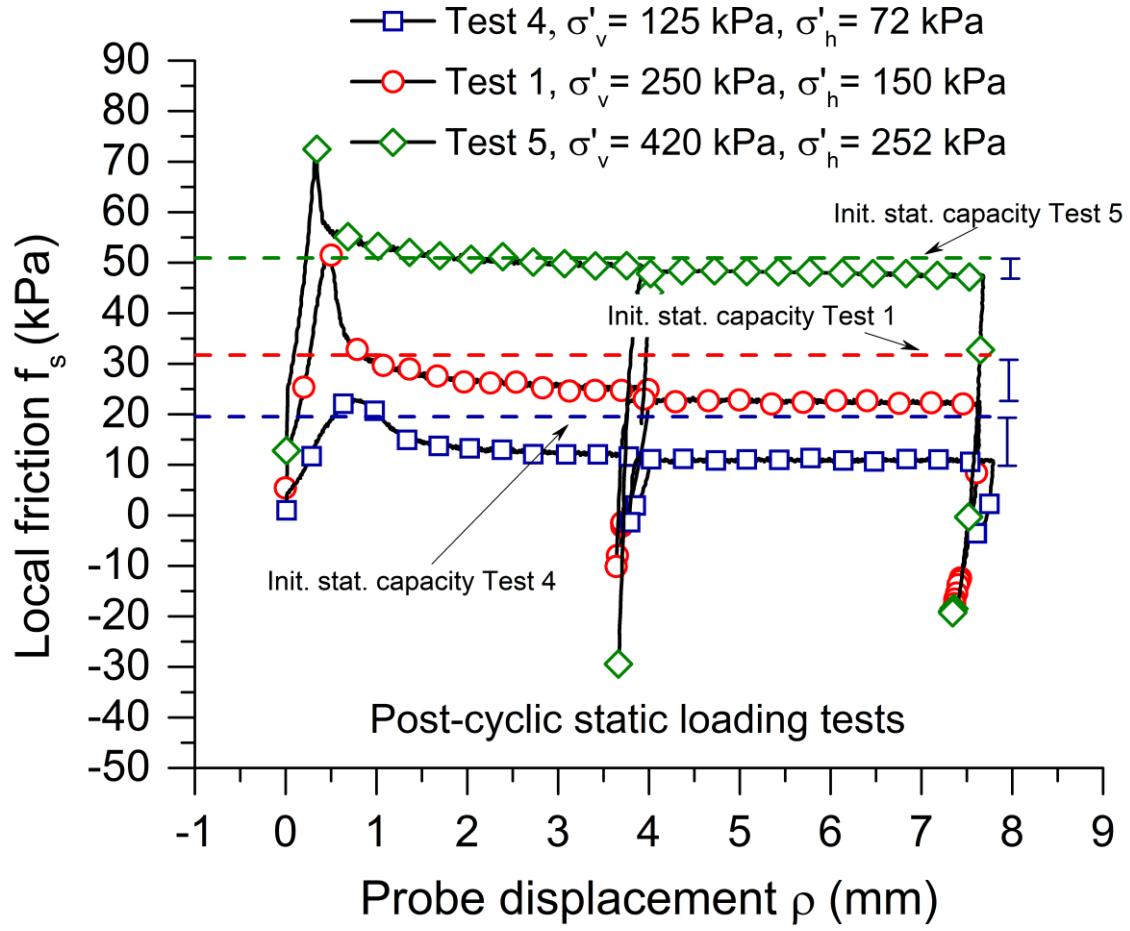


Fig. 17. Influence of initial effective consolidation stress level on the evolution of local friction upon post-cyclic static loading phases

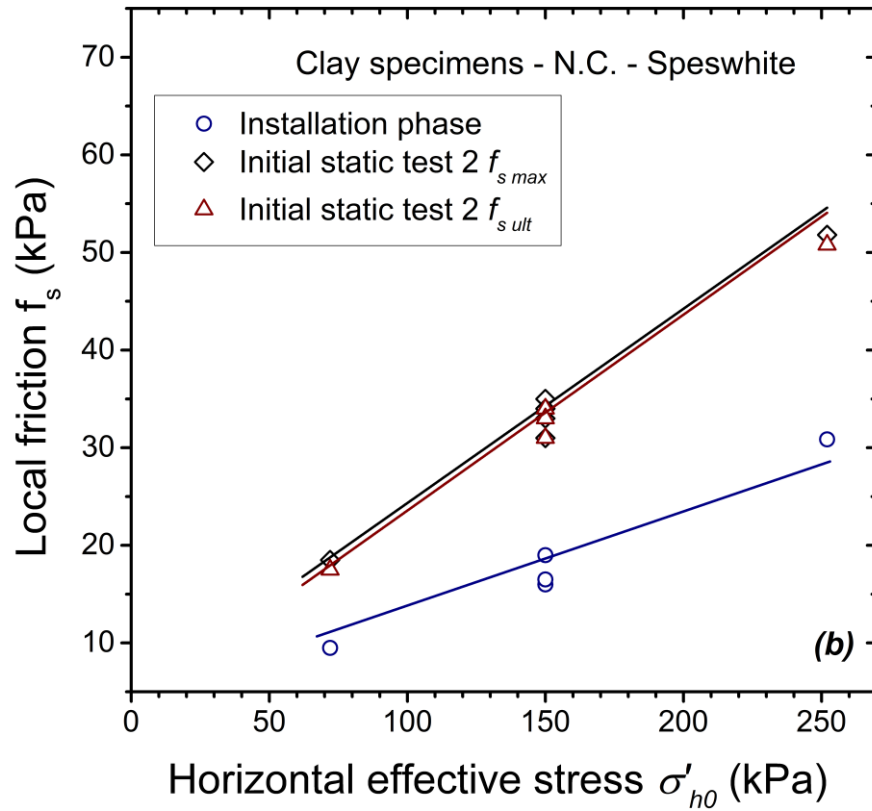
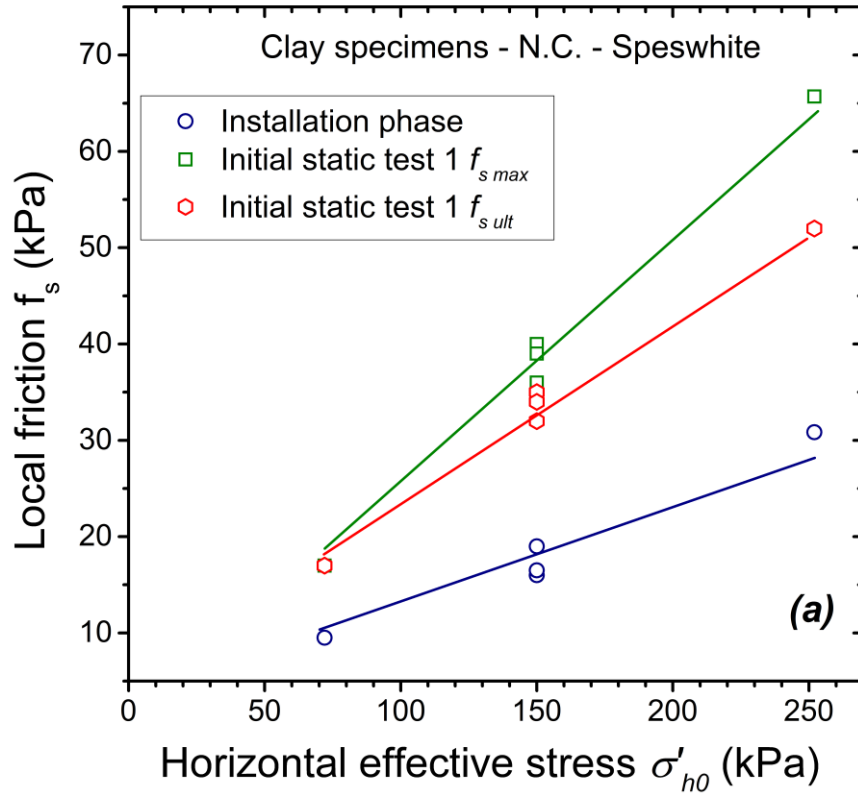


Figure 18. Synthesis of maximum and ultimate values of local friction upon: (a) 1<sup>st</sup> pre cyclic static tests and (b) 2<sup>nd</sup> pre cyclic static tests compared to the maximum mobilized friction upon installation phase

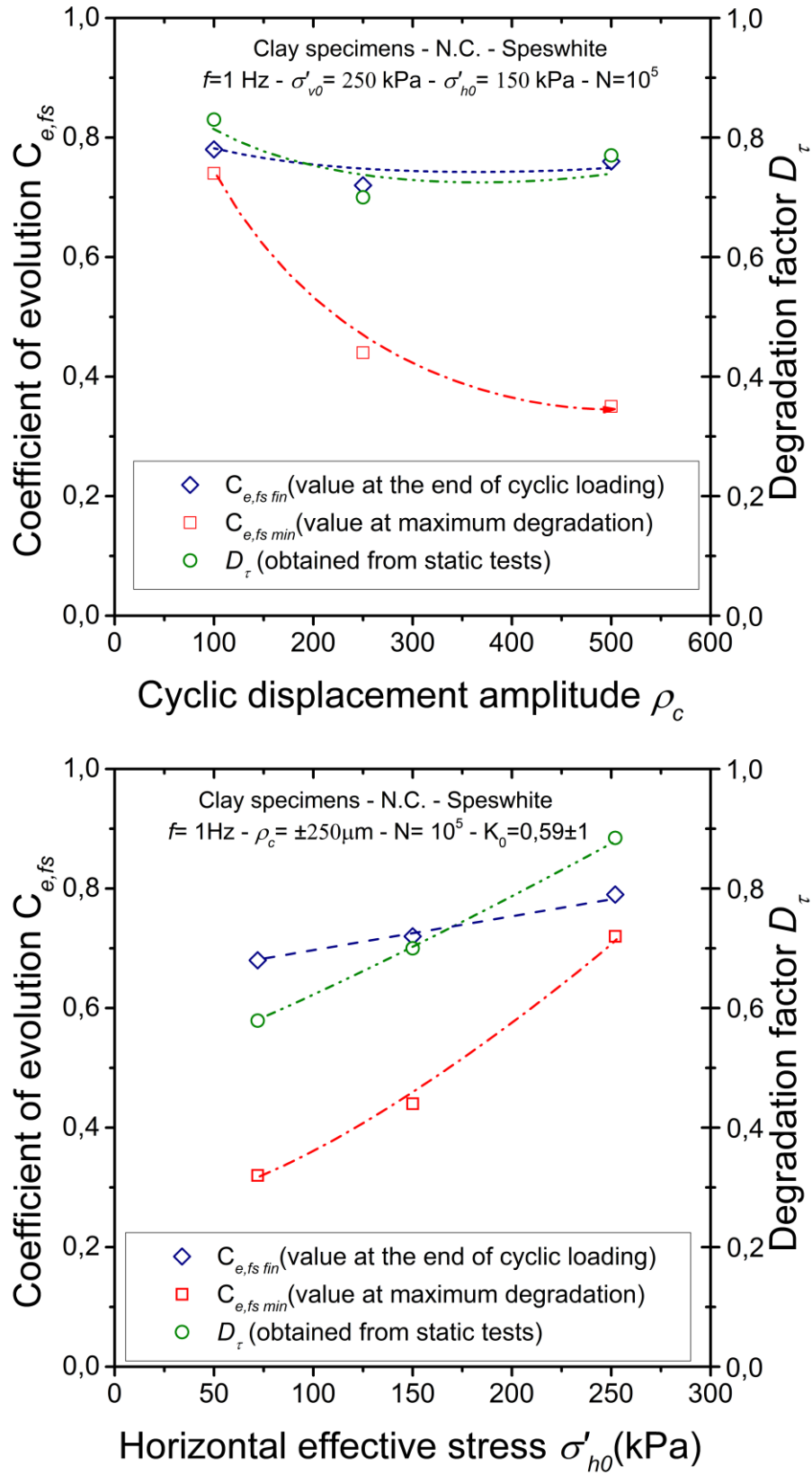


Figure 19. Synthesis of the effect of cyclic displacement amplitude and effective horizontal stress on coefficient of evolution  $C_{e,fs}$  and degradation factor  $D_\tau$

## A parametric study on the evolution of cyclic clay-pile interface friction for large numbers of cycles

### Tables

Table 1. Physical properties of Speswhite kaolinite

Mineralogy	Liquid limit (%)	Plastic limit (%)	Plasticity index (%)	Specific gravity (g/cm <sup>3</sup> )	Percentage finer than 10 $\mu$ m (%)
kaolinite	58	28	30	2,64	98

Table 2. Main characteristics of tests performed

Test identification	$\sigma'_{v0}$ (kpa)	$\sigma'_{h0}$ (kpa)	Frequency $f$ (Hz)	Cyclic amplitude $\rho_c$ ( $\mu$ m)	Number of cycles	Observations
Test 1	250	150	1	$\pm 250$	100 000	Reference test
Test 2	250	150	1	$\pm 100$	100 000	Effect of amplitude
Test 3	250	150	1	$\pm 500$	100 000	Effect of amplitude
Test 4	125	72	1	$\pm 250$	100 000	Effect of initial state
Test 5	420	252	1	$\pm 250$	100 000	Effect of initial state

Table 3. Synthesis of the results in term of coefficient of evolution and the degradation factor

Test identification	$\sigma'_{v0}$ (kPa)	$\sigma'_{h0}$ (kPa)	Frequency	Cyclic amplitude	Number of cycles N	$C_{efs}$		$D_\tau$
			$f$ (Hz)	$\rho_c$ ( $\mu$ m)		maximum degradation	at the end of cyclic test	
Test 1	250	150	1	$\pm 250$	100 000	0,44	0,72	0,70
Test 2	250	150	1	$\pm 100$	100 000	0,74	0,78	0,83
Test 3	250	150	1	$\pm 500$	100 000	0,35	0,76	0,77
Test 4	125	72	1	$\pm 250$	100000	0,32	0,68	0,58
Test 5	420	252	1	$\pm 250$	100000	0,72	0,79	0,88